Bone 119 (2019) 19–35

Contents lists available at ScienceDirect

Bone

journal homepage: www.elsevier.com/locate/bone

Review Article

Imaging methods used to study mouse and human HSC niches: Current and emerging technologies

Gavin Tjin[a,1], Eugenia Flores-Figueroa[b,1], Delfim Duarte[c,d,1], Lenny Straszkowski[a], Mark Scott[c,e], Reema A. Khorshed[c], Louise E. Purton[a,f,*], Cristina Lo Celso[c,d,**]

[a] St Vincent's Institute of Medical Research, Fitzroy, Victoria, Australia
[b] Oncology Research Unit, Oncology Hospital, National Medical Center Century XXI, Instituto Mexicano del Seguro Social (IMSS), Mexico City, Mexico
[c] Department of Life Sciences, Sir Alexander Fleming Building, Imperial College London, London, UK
[d] The Sir Francis Crick Institute, London, UK
[e] Institute for Molecular Bioscience, University of Queensland, Brisbane, Australia
[f] The University of Melbourne, Department of Medicine at St Vincent's Hospital, Fitzroy, Victoria, Australia

ARTICLE INFO

Keywords:
Imaging
Bone
Niches
Hematopoiesis
Leukemia

ABSTRACT

Bone marrow contains numerous different cell types arising from hematopoietic stem cells (HSCs) and non-hematopoietic mesenchymal/skeletal stem cells, in addition to other cell types such as endothelial cells- these non-hematopoietic cells are commonly referred to as stromal cells or microenvironment cells. HSC function is intimately linked to complex signals integrated by their niches, formed by combinations of hematopoietic and stromal cells. Studies of hematopoietic cells have been significantly advanced by flow cytometry methods, enabling the quantitation of each cell type in normal and perturbed situations, in addition to the isolation of these cells for molecular and functional studies. Less is known, however, about the specific niches for distinct developing hematopoietic lineages, or the changes occurring in the niche size and function in these distinct anatomical sites in the bone marrow under stress situations and ageing. Significant advances in imaging technology during the last decade have permitted studies of HSC niches in mice. Additional imaging technologies are emerging that will facilitate the study of human HSC niches in trephine BM biopsies. Here we provide an overview of imaging technologies used to study HSC niches, in addition to highlighting emerging technology that will help us to more precisely identify and characterize HSC niches in normal and diseased states.

1. Introduction

We make billions of mature blood cells every day by highly defined processes involving the commitment and differentiation of blood-forming stem cells (hematopoietic stem cells, HSCs). Numerous different steps are required for an HSC to become a mature blood cell and these occur in the bone marrow (BM), in specialized BM microenvironments (aka niches). The niches are largely composed of non-blood cells, including cells that form bone, and there are specific niches for primitive cells, including HSCs and progenitors, in addition to all of the different maturing blood cell lineages [1,2].

There are numerous types of niche cells in the BM in human and mouse. Most of what we know about these niche cells have arisen from studies using mouse models. Numerous excellent reviews are available that provide extensive overviews of the distinct cell types that comprise HSC niches, recent ones include those by Crane et al. [3] and Gao et al. [4]. The purpose of this current review is to discuss the different imaging technologies that are currently being used to study HSC niches in human and mouse samples. Nevertheless, a basic overview of different cell types that contribute to bone marrow niches is provided here.

There are a range of osteoblast lineage cells present in BM, ranging from the most immature skeletal stem cells, osteoprogenitors, osteoblasts, which are found on the bone (endosteal) surface, to the most mature osteocytes, which are embedded in the bone [5]. Perivascular cells, which line arteries in the bone marrow, include MSCs that are derived from two separate sources: neural crest-derived Nestin (Nes)-expressing MSCs [6] and mesenchymal limb bud-derived Prx1-expressing MSCs [7,8]. Nes+ MSCs cannot form adipocytes [9,10]. In contrast, progeny of the Prx1+ MSCs include leptin receptor+ (LepR+) mesenchymal cells [9] and CXCL12-abundant reticular (CAR) cells

* Correspondence to: L.E. Purton, 9 Princes St, Fitzroy, Vic 3065, Australia.
** Correspondence to: C. Lo Celso, Imperial College London, Fleming Building, South Kensington Campus, Exhibition Road, London SW7 2AZ, UK.
E-mail addresses: lpurton@svi.edu.au (L.E. Purton), c.lo-celso@imperial.ac.uk (C. Lo Celso).
[1] Equal first authors.

https://doi.org/10.1016/j.bone.2018.04.022
Received 27 February 2018; Received in revised form 23 April 2018; Accepted 23 April 2018
Available online 25 April 2018
8756-3282/

[9,11], the latter which have been shown to be the source of all adipocytes in BM [9].

Endothelial cells line all blood vessels in the body and in the BM they form a barrier between the developing hematopoietic cells and the blood. The two major types of blood vessels in BM are sinusoids and arterioles [10,12]. The arteriolar vessel types are lined by perivascular cells, such as osteoprogenitors or smooth muscle cell alpha-expressing cells. Furthermore, arteriolar vessel types consist of $CD31^{high}$ $endomucin^{high}$ type H endothelial cells, which are located in the metaphysis and near the endosteum, and connect to $endomucin^{-ve}$ arterioles [12]. BM sinusoids (also referred to as $CD31^{low}$ $endomucin^{low}$ Type L vessels) [12] are more permeable than BM arterioles [10] and are associated with different mesenchymal cell types, such as LepR+ cells and some of their progeny.

2. Approaches used for the visualization of bone marrow niches in mice

The use of genetically modified mouse models has enhanced the study of phenotypic murine HSCs and the manipulation of specific niche cells, such as deletion of specific niche regulatory factors. The many transgenic mouse lines used in HSC and HSC niche research were previously reviewed by Joseph et al. [13]. Updates of additional mesenchymal transgenic mice that have been generated more recently are provided in an accompanying review by Green et al. in this edition of Bone [14]. These mice, combined with fluorescent reporter mice, have been very useful for many imaging studies investigating HSC niches.

2.1. Fluorescent reporter mice

The use of fluorescent reporter mice to detect different cell types in vivo have become a gold standard tool for imaging studies investigating interactions of different niche cells and hematopoietic cells. There are an increasing number of transgenic mice being made that have reporters in which a fluorescence protein (most commonly green fluorescence protein, GFP) is driven by or fused to the gene of interest and hence only cells that express that gene are fluorescent (for example, Col2.3-GFP [15], nestin-GFP [16], *Osx1*-GFP [17]) [18] and Flk1-GFP [19]). In addition, numerous transgenic Cre lines have been generated without a fluorophore, but can be used for imaging by crossing the Cre transgenic mouse to a fluorescent reporter mouse. The most commonly used are the *Rosa26* (*R26*) reporter strains previously discussed in Joseph et al. [13]. The largest limitation of these latter reporter strains for use in imaging studies is that all progeny of the cell that is targeted by the Cre transgene will be detected by the fluorescent reporter, as discussed in Green et al. [14].

2.1.1. GFP and RFP based fluorophores

GFP was first isolated from the jellyfish *Aequorea victoria* [20] and since then further research on the DNA encoding the protein has generated a series of fluorophores that have enhanced emission intensity and stability compared to the first generation GFP. Some of the most well-known fluorophores that are derivatives of GFP are yellow fluorescence protein (YFP), cyan fluorescence protein (CFP) and the enhanced versions of these latter two, which are brighter and more photostable fluorochromes [21]. The advantage of GFP is its ability to be spontaneously fluorescent when produced by the cells, hence the formation of chimeric GFP fusion proteins through genetic engineering allows for the visualization and localization of proteins of interest within the cells in real-time. However, while many derivatives of the GFP molecule are available, the emission maxima of these fluorescent proteins are limited in the red fluorescence. The discovery and isolation of the red-fluorescent protein (RFP) from the discosoma coral [22] was therefore a significant step forward for imaging studies.

RFP and RFP-derived fluorophores have emission in the red range [23] which complements with the GFP fluorophores. Furthermore, as native autofluorescence of cells and tissue is typically in the green-yellow range, RFP suffers from less issues with spectral overlap with autofluorescence, allowing it to be visualized much more easily compared to GFP which emits in the autofluorescence range. Both GFP and RFP can be used in tandem to tag multiple proteins of interest and visualizing the interactions between them. Recently, far red-shifted fluorescent proteins have been generated, with the aim to increase the palette of fluorophores available. mCherry, neptune, crimson, plum and Katushka are examples of such proteins and are reviewed by Chudakov et al. [24].

2.1.2. Multicolored reporter strains

Multicolored reporter strains such as *R26R*-Confetti mice [25], HUe mice [26] and Rainbow mice [27] are increasingly being used in imaging studies of HSCs and microenvironment cell types. A "*Zebrabow*" rainbow zebrafish reporter has also recently been generated [28].

The Brainbow 2.1 mice [29] were generated to study lineage tracing in the brain, producing at least 90 colors in vivo. The *R26R*-Confetti mice are a modified version of the Brainbow 2.1 mice, where four fluorescent proteins (GFP, YFP, RFP and CFP) were inserted into the ubiquitously expressed *R26* locus, with a LoxP "stop" site inserted upstream of the *R26* locus. Upon Cre activation, the LoxP site is excised and recombination occurs in a random fashion to permit one of the four colors to be expressed by the Cre-targeted cell [25].

A similar approach has led to the recent generation of another transgenic mouse strain (HUe) in which four fluorophores (GFP, EYFP, tDimer2 and Cerulean) are driven by a ubiquitously expressed chicken actin promoter [26]. The HUe reporter strain has approximately 20 tandemly integrated cassettes, theoretically producing over 1000 different colors in the red, blue and green hues permitted by the fluorophores. In contrast, the Rainbow mice, in which the fluorophores are also driven by the chicken actin promoter, harbors three fluorophores (EGFP, ECFP and mRFP1) [27]. The *Zebrabow* fish also has three fluorophores: RFP, CFP and YFP [28].

There are some caveats associated with the use of these multicolored reporter animals. One is the dominance of some of the colors over others, which can vary from tissue to tissue. For example, in the *R26R*-Confetti reporter, the GFP (which is nuclear) is not expressed very well by the marked cells [25] (and Purton lab, unpublished observations). The RFP (which is cytoplasmic) is very bright in both imaging and FACS studies, with YFP (which is also cytoplasmic) also being readily detectable. The CFP is membrane associated and weaker to detect using both FACS and imaging methods, but is nevertheless detectable. For FACS studies, significant effort is required to compensate between GFP and YFP, however, with appropriate filters, this is possible to achieve. Finally, the number of colors that can be expressed is reliant on whether the reporter is heterozygous or homozygous: for example, if the R26R-Confetti genotype is heterozygous only four colors can be expressed, however, if homozygous then 10 different color combinations are possible [30]. This is especially important to recognize if using these reporter mice for studies incorporating FACS, particularly if combining the use of antibodies with the fluorophores to detect different cell types.

Recent studies have used these different multicolored reporter mice to investigate properties of bone marrow niche cells, including bone marrow vasculature using *R26R*-Confetti mice [31], mesenchymal lineage cell populations using Rainbow mice [32] and HSCs and mesenchymal lineage cell populations using HUe mice [26]. Furthermore, the *Zebrabow* fish have been used to study clonal hematopoiesis from HSCs [28].

2.2. Challenges linked to fluorescence immunostaining

While multicolored reporter mice allow clonal analyses within the targeted cell population, lineage or cell type-specific fluorophores must be combined to simultaneously observe combination of cells. This is

particularly challenging for the study of HSC niches, as lineage reporters are limited and most often only available as GFP, or requiring complex breeding strategies to intercross them. Antibodies conjugated to a variety of fluorophores are the ideal tool when several markers need to be combined to identify HSCs and niche components. As is the case for flow cytometry (FACS), there are numerous different antibodies that can be used to detect distinct niche cell types and HSCs on tissue sections. However, this approach too presents significant challenges. The largest limitation of fluorescence microscopy compared to FACS is the number of fluorophores that can be simultaneously imaged within a single sample. While it is routine to detect cells that have been simultaneously stained with > 10 fluorophores using FACS, it becomes exponentially more difficult after 4 colors with every additional fluorophore using standard fluorescence microscopy.

As the number of fluorophores within the experiment grows, the fluorescence emission spectra of the fluorophores starts to overlap and the signal from adjacent fluorophores are then detected in the detector dedicated to a neighboring fluorophore, an event known as spillover. One of the techniques employed to distinguish between overlapping fluorescence profiles is fluorescence compensation, which is a requirement for FACS [33] but is not easily performed for fluorescence microscopy. This originates from the difference in the acquisition protocol and post-processing capability of the two techniques.

Fluorescence compensation for FACS is simple to perform as all of the cells are in suspension and hence the data is acquired for each individual cell. However, in a tissue one must first be able to distinguish between each cell and the boundaries between them in order to obtain fluorescence emission profile for each individual cell. This is made more difficult by the fact that cells in tissue sections exist in 3D with multiple cells stacked on top of each other. When sectioning the tissue for imaging studies, each section will cut through some of the cells and thus only parts of cells may be present within the image. Furthermore, for accurate compensation a large sample number is required, this is particularly difficult for rare cell populations. For FACS, millions of cells can be analyzed within a short period of time, however fluorescence microscopy is limited to analysis within the field of view which, depending on the magnification and cell density, can contain anywhere between dozens to hundreds of cells. While lower magnification images can be taken one must consider the resolution of the image as it must be high enough to resolve individual cells within the image; this is not a problem for FACS as analysis is done for each individual cell.

Another challenge to consider for fluorescence imaging is the sample preparation. Most samples for fluorescence imaging are either formalin fixed paraffin embedded tissues (FFPE) or fresh frozen tissues. Fixed samples can be stored for an extended period of time and thus allow for analysis of historical samples. Most pathological samples are stored as FFPE samples and due to the process of fixation, there are inevitable changes to the epitopes on the sample, requiring additional steps to unmask the epitopes for the target protein of interest [34]. Additionally, the fixation process often increases the level of autofluorescence within the tissue, compounding an already prominent problem as tissue samples have high levels of autofluorescence due to numerous proteins having inherent fluorescence [35]. As a result, signal amplification is often required in immunofluorescence protocols to overcome this issue.

Signal amplification can be achieved through several techniques. A common method is to use indirect labelling using fluorophore conjugated secondary antibodies against the primary antibody for a modest signal amplification (multiple secondary antibodies can bind to a single primary antibody). Further signal amplification can be achieved through the avidin biotin complex (ABC) signal amplification whereby the primary/secondary antibody is conjugated to a biotin molecule that will form a complex with multiple fluorophore-conjugated avidin molecules. However, for the purposes of fluorescence multiplexing, these indirect signal amplification techniques are of limited utility. If multiple primary antibodies are raised in the same species and are of the same isotype, the secondary antibody will not be able to distinguish between each of these primary antibodies on a single section. The ABC signal amplification also presents with the same problem as the complex will form for any antibody complexed with biotin. Even combining these two techniques will only amplify two of the markers in the panel, leaving directly conjugated primaries or the need for antibodies raised in different species as the remaining option. However, until very recently, these limitations using antibody-based approaches have restricted many of the imaging studies that have been performed to date to four colors. One of the most exciting to overcome this limitation is the use of tyramide signal amplification (TSA) in immunofluorescence.

2.2.1. Overcoming antibody species limitation in fluorescence immunolabeling with tyramide signal amplification (TSA)

Tyramide molecules are converted into a highly oxidized free radical in the presence of peroxidase (i.e. horseradish peroxidase) and hydrogen peroxide, causing it to covalently bond with tyrosine residues adjacent to the peroxidase. Through the conjugation of tyramide with fluorophores, the deposition of a vast number of fluorophores onto the site of antibody binding is possible, achieving signal amplification that is far superior to even the ABC system and in fact can be done in tandem with other signal amplification protocols because TSA is a modification of the reaction product and not the detection system [78].

Additionally, the deposition of fluorophores by TSA is achieved through covalent binding and thus is permanent [78]. This allows the sample to be "stripped" of the antibody used for the detection of the marker without affecting the fluorophore, unlike other amplification methods whereby the "stripping" process would also strip the fluorophores from the sample. This permits fluorescence multiplexing by sequential antibody labelling and stripping with the TSA using tyramide molecules conjugated to different fluorophores. The end result achieves signal amplification for all labels within the panel with signal intensities brighter than any other signal amplification protocols (Fig. 1). Furthermore, because antibodies from the previous sequence have been

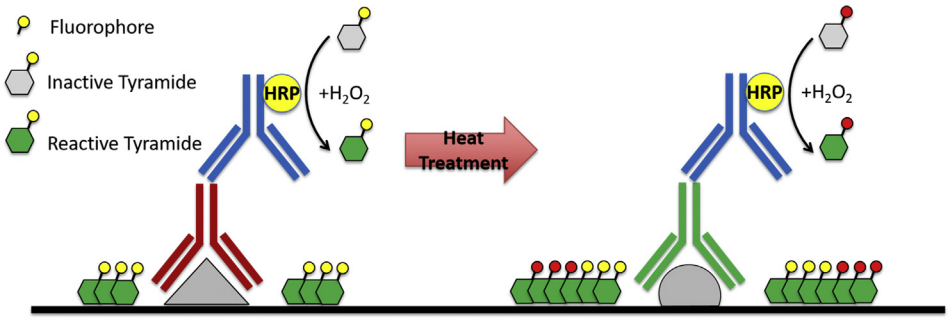

Fig. 1. Tyramide signal amplification for multiplexed immunofluorescence. The primary antibody (red) complex containing HRP catalyzes the formation of reactive tyramide molecules that form covalent bonds with tyrosine residues in the tissue. Subsequent heat treatment/heat induced antigen retrieval removes the primary antibody complex while retaining fluorophore-conjugated tyramide molecules bound to the tissue and primes the tissue for the next primary antibody complex to detect a different epitope. The process is repeated until all targets of interest have been labelled with fluorophore conjugated to tyramide. Abbreviations: HRP = horseradish peroxidase, H_2O_2 = hydrogen peroxide. (For interpretation of the references to color in this figure legend, the reader is referred to the web version of this article.)

removed prior to subsequent antibody labelling, antibody species limitations found with indirect signal amplification methods no longer apply and antibodies from the same species/isotype can be used and amplified equally [79].

The development of the TSA technique allowed for the potential of fluorescence microscopy to catch up with FACS in the number of markers that can theoretically be labelled. However, this has still not resolved the issue of fluorescence spectral overlap when working with multiple fluorophores, and fluorescence compensation still remains a challenge on tissue samples. Recent developments with this technology have overcome this limitation through a technique known as spectral imaging combined with linear unmixing which are discussed in Section 6 further below in this review.

3. Sample preparation for imaging tissue sections in both 2D and 3D

The optimization of the samples from harvest to immunohistochemistry (IHC) interpretation is essential for accurate quantitation of the different proteins of interest, including markers for HSCs and bone marrow microenvironment cell types. The IHC protocol begins from sample preparation and it is one of the most important steps in the experiment. Optimized and standardized sample preparation allows for the acquisition of reliable and reproducible results. Different tissues require distinct processing protocols. An overview of important parts of the bone processing is provided below.

3.1. Tissue preparation

Adequate fixation of bone tissue is essential prior to processing and embedding the samples [36,37]. Under- or over-fixation can be detrimental to the tissue, as antigen degradation may occur and therefore affect antibody-epitope/antigen binding [36–38]. Inadequately processed tissue will also pose problems when sectioning and staining samples [36]. Histopathology workflow requires bone to be decalcified as a fundamental procedure, with various decalcifying solutions available [39]. Many factors may influence the decalcification process and tissue infiltration, such as skin or muscle attached to the bone, bone size, and the type of decalcifying solution used [40]. Morphology and antigenicity may be negatively impacted if the decalcification process is not carried out correctly [37], therefore proper decalcification is paramount for successful sectioning and IHC staining.

3.2. The importance of control sections

The detection of specific proteins such as antigens within or on the surface of specific cell types, or tissue architecture such as vasculature is conducted via IHC [38,41]. Due to the nature of this technique and subjectivity, having appropriate positive and negative controls is critical for the valid and accurate interpretation of IHC results [41]. The method used to detect and amplify the protein of interest and promote antibody-antigen binding is another variable to be considered when interpreting results [36,38].

Non-specific binding of an antibody may result in false-positive interpretation; therefore, the use of a negative control is of utmost importance [38,41]. Omitting the primary antibody as a negative control is not a valid method to accurately assess primary antibody-epitope binding specificity. Primary antibody omission is only indicative of the secondary antibody binding non-specifically to the section [38,41]. To validate specific primary antibody-epitope binding, a suitable negative control would be a serum or immunoglobulin that is isotype specific to your primary antibody [41] and ideally, although rarely available, sections of tissues known not to express the antigen studied, such as sections from knock out animals.

4. Imaging in 2 dimensions: studies of thin tissue sections

4.1. Histomorphometry-based approaches for quantitation of bone marrow niches

Histomorphometry involves the quantitative analysis of the microarchitecture of a tissue section. It is a gold standard imaging technology used to quantitate bone [42] in addition to other components of the bone marrow microenvironment, such as blood vessels [43]. There are different software packages that can be used to quantitate the bone microenvironment, such as ImageJ (and its plugin, BoneJ) or OsteoMeasure. The quantitation of bone parameters including osteoid is commonly performed using undecalcified plastic-embedded samples, and has been extensively reviewed by Dempster et al. [42]. Quantitation can also be performed using decalcified bones, in particular when combined with immunohistochemistry (IHC) to detect specific cell types [43,44].

OsteoMeasure (OsteoMetrics, Atlanta, GA, USA) is the most commonly used software designed for histomorphometry analyses, and it is used predominantly in the bone and musculoskeletal fields [45,46]. OsteoMeasure software links a real-time view of a stained sample under a microscope, and sends this information to a computer tablet via a camera [45]. A pen detected by the tablet can then be guided by the user to identify the cells of interest, or trace around cells or structures (such as vessels) within a sample to obtain information on the cell size, perimeter and cell number.

Using OsteoMeasure, locating a region of tissue for analysis can be done in real-time, using structures or landmarks inherent to the tissue (Fig. 2). The production of trabecular bone occurs via a process called endochondral ossification [47]. This is a complex, finely regulated process involving crosstalk between chondrocytes, osteoblast lineage cells, osteoclasts and endothelial cells [48]. During this process, cartilage is initially formed, and then gradually becomes replaced by bone, with a combination of mineralized bone tissue and cartilage forming the primary spongiosa [47]. The primary spongiosa is located just below the growth plate as indicated by the green box in Fig. 2. The secondary spongiosa is located just below the primary spongiosa, as shown by the red squares arranged in a grid pattern (Fig. 2). The secondary spongiosa is a standard area in which measurements are made for comparable analyses across multiple samples. These landmark regions are easily identifiable and provide a consistent comparison of the same region across samples.

OsteoMeasure allows the user to trace regions of interest such as the volume of blood vessels (sinusoids), trabecular bone, and adipocytes, as well as manually quantifying the numbers of vessels or cells of interest (Fig. 3) [5]. OsteoMeasure will calculate the volume and area of defined regions, the cell or tissue perimeter, and the numbers of cells or vessels counted manually by the user [45] (Fig. 3). Expertise is required in identifying various structures and differentiating the cell types by the user, which can be aided by IHC (Fig. 3). This technique is labor intensive as it requires the user to visually identify and manually demarcate areas of interest as demonstrated in Fig. 3 [46]. Accurate identification of cell types and structures is underpinned by robust/specific reproducible IHC staining.

The applications of this software are broad, with respect to quantification of various cell types and niches, therefore the use of OsteoMeasure can be applied in many fields. Other open-source software such as Image J can also be utilized to write specific programs and tailor the analyses towards specific stains to identify particular cell types [46]. We have recently used this approach to show that endosteal vessels are remodeled in patients with AML [49].

4.2. Imaging in 2 dimensions: tissue arrays for the study of hematopoiesis

Tissue arrays consist of at least two different specimens in one slide, but the number of specimens installed can go up to the hundreds. One

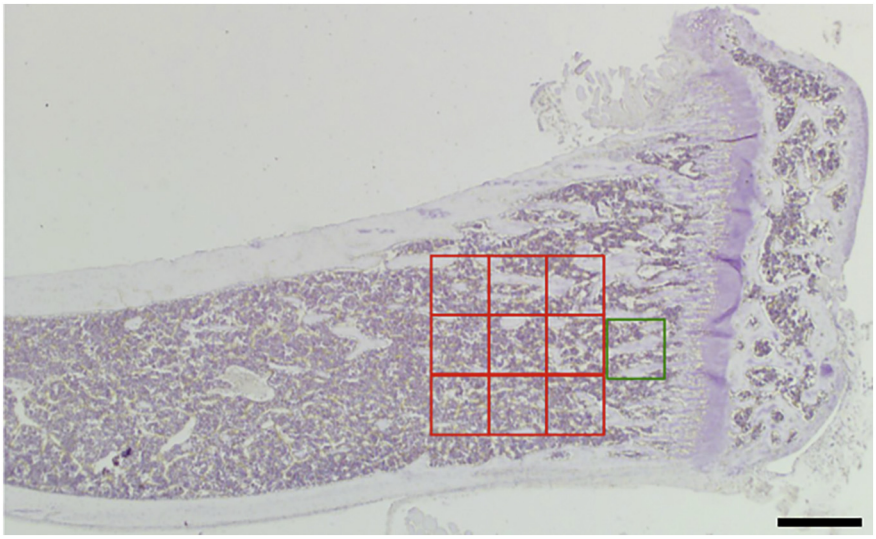

Fig. 2. Spatial localization of OsteoMeasure fields. Shown is a mouse tibia cut at 5 μm, stained with vascular endothelial growth factor 3 (VEGFR-3), amplified using 3,3′-diaminobenzidine (DAB) and counter-stained with hematoxylin, original magnification 4×. The primary spongiosa is indicated by the green box and the secondary spongiosa regions by the red boxes. The primary spongiosa is used as a reference point for locating the secondary spongiosa, which is the common site of measurement for different bone marrow niche cell types and tissues including osteoblasts, trabecular bone and blood vessels. Scale bar = 500 μm. (For interpretation of the references to color in this figure, the reader is referred to the web version of this article.)

of the main purposes of a tissue array is to perform a simultaneous and standardized study of two or more samples, hence it has been generally used along with IHC to validate and/or discover protein biomarkers. Tissue arrays are not restricted to protein studies; they can also be used to analyze nucleic acids [50]. Tissue arrays have been used in the research of solid tumors [51], but are not limited to those, as they can be successfully used for the study of hematologic diseases [52,53]. Tissue arrays are useful for studying hematopoiesis and hematopoietic disorders; they can be built from different hematopoietic organs, such as spleen, bone marrow and thymus; and they can also be built from suspensions of hematopoietic cells [54]. Tissue arrays from bone marrow require special technical consideration [52], as they may contain two or three types of tissue including cortical or trabecular bone, cartilage and bone marrow stroma.

4.2.1. Types of tissue arrays

There are many types of tissue arrays and many methods of construction [55]. According to the size of the specimen, there are two main categories, tissue macroarrays (also called tissue arrays) and tissue microarrays (TMA). Tissue macroarrays consist of entire organs (from mouse or other small species), human biopsies or small pieces of tissue. The number of samples per slide is limited, due to the size of the specimens, for example; tissue macroarrays from mouse hematopoietic tissues can contain up to five or 6 spleens, femurs, tibiae or pelvises (Fig. 4).

Tissue macroarrays can be built by placing different samples that have been embedded separately (referred to as single specimens on Table 1) onto one slide after cutting, or from tissues that have been embedded together (Fig. 4). In either case, it is important to include a small piece of a different tissue (as a marker), to control the orientation of the slide and track the identity of the tissues (Fig. 4). This tissue can also be used as a control tissue for the stain.

In contrast, tissue microarrays (TMA) can contain hundreds of samples, but the size of each sample is limited. TMA are very useful for finding or validating biomarkers that have been identified by genomics or proteomics, as they allow the simultaneous staining and scoring of a large number of samples.

The most commonly used core size for TMA varies from 0.6 mm to 1 mm (Fig. 5). It is important to consider the histology of the tissue and the representation of the area included in the core. TMAs will leave a hole in the original block; this has to be taken in consideration when diagnostic human samples are being used to build them (Table 1). TMA

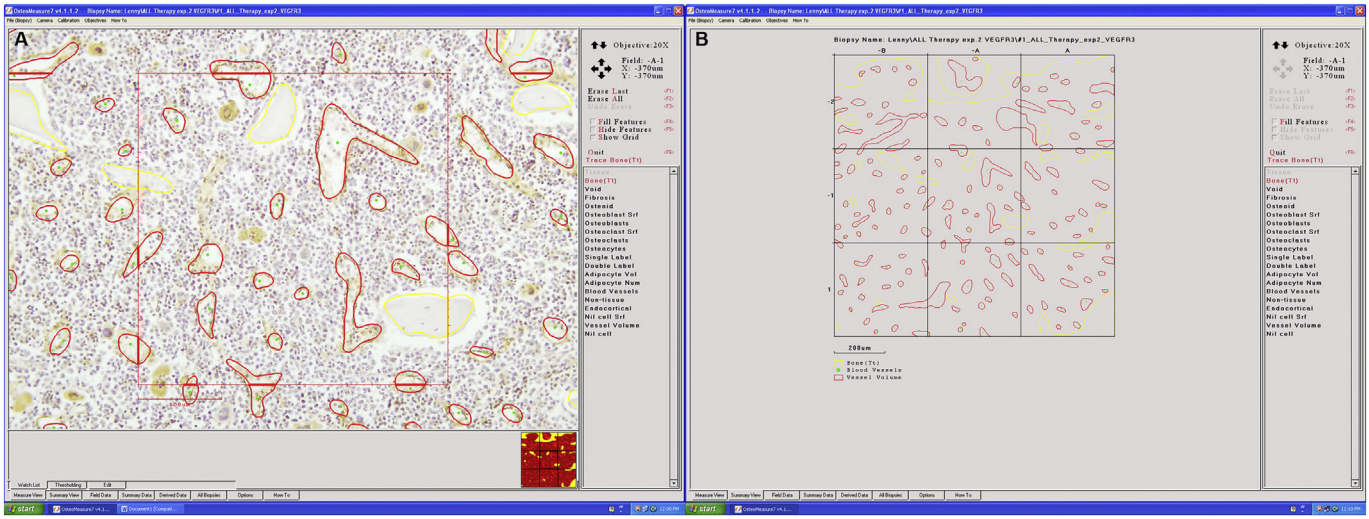

Fig. 3. OsteoMeasure user interface. This image is of a mouse tibia stained with VEGFR-3 to detect BM sinusoids at 20× magnification. A) The BM sinusoids were traced and are outlined in red, the trabecular bone is traced and outlined in yellow. B) A summary view of traced regions. (For interpretation of the references to color in this figure legend, the reader is referred to the web version of this article.)

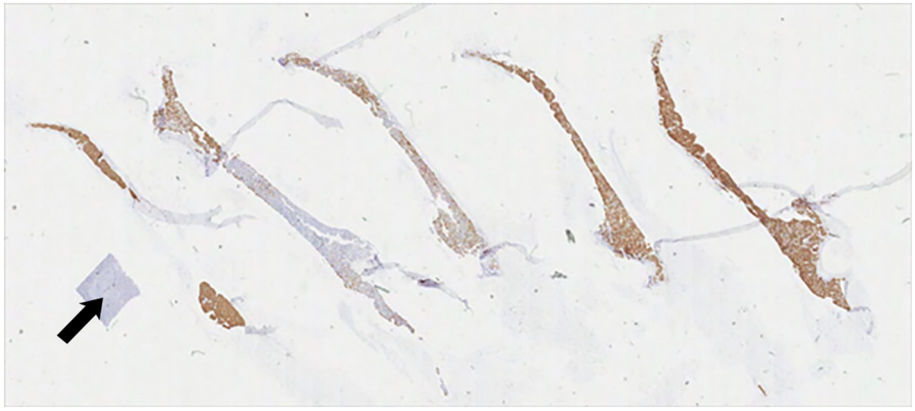

Fig. 4. An example of a tissue macroarray. Photomicrograph of a tissue microarray (4 μm sections) that included five xenografted mouse pelvises. The slide has been stained by immunohistochemistry with an anti-human CD45 antibody (detected using 3,3′-diaminobenzidine, DAB) and counterstained with hematoxylin. The array included one small piece of normal mouse spleen (black arrow) to control the orientation of the slide and the identity of the specimens. The normal mouse spleen was also used as a negative control for the anti-human CD45 antibody. The slide has been digitalized using an Aperio CS2 scanner.

can be built from paraffin embedded or frozen tissue [55]. Decalcification of the bone is required when using human bone marrow trephines or mouse bone samples.

4.2.2. Tissue array planning and quality control

The first step in building a tissue array is to select the type of array that works best for your experiment. To be taken in consideration are the size of the specimen, the importance to preserve the original block intact, the size of the area of interest and the number of samples to be included (Table 1).

The second step is to build a tissue array map or TMA map, including control tissue that facilitates the orientation of the block and the slide, and preserves the identity of the samples. The control tissue can also be used as a positive or negative control of the stain (Figs. 4 and 5). It is important that all of the samples included on the tissue array have the same fixation and decalcification protocol. The tissue array can contain only controls or experimental groups, or can be a mix of both. The TMA map should include a duplicate or triplicate of each sample that will be identified with a consecutive number, including the code of the sector (see S1–S4 in Table 2) and the number of samples, (e.g. 101 refers to the first sample of sector 1, 201 refers to the first sample of sector 2 in Table 2). It is important to maintain the orientation when placing the cut tissue onto the slide, hence asymmetric sectors are recommended to assist with this.

The map needs to contain a code for each sample; samples can be arranged in sectors (S1–S4). Sectors are best to be arranged in an asymmetric format, which helps the histotechnologists to place the cut section in the right orientation according to the map. Control tissue can help with both orientation and to function as a positive or negative control of the stain.

The quality control of the tissue array includes an evaluation of a slide consisting of a 4 μm hematoxylin and eosin (H&E) stained section representative of the array. The H&E stain will determine if the tissue has been preserved and if the area of interest is represented, or if there are some areas missing or with artifacts (Fig. 6). In order to avoid artifacts, it is important to embed the samples on the flattest side and to keep the tissue at the same level. If the block is going to be used extensively, it is recommended to include a slide stained with H&E that is obtained on the 10th cut of each block.

The problem of having too much bone or cartilage (if analysis of bone marrow is being performed) can be minimized by carefully marking the representative areas in the bone marrow samples and by punching the selected areas exactly [52] (Fig. 7A and B). Each spot needs to assessed and missing or empty spots (Fig. 8A) or spots with artifacts have to be discarded from the analysis, empty spots usually account for < 5% of the spots [52]. Spots that do not have representative areas also need to be discarded (Fig. 8B and C). If the TMA shows only muscle, sometimes a deeper cut can solve the problem (Fig. 8C). It is expected that between 10% and 20% of the cores will not be suitable for evaluation [52,53].

One of the most critical steps for building a tissue array from bone marrow is the selection of the cores. Smaller cores (0.6 mm) are usually less likely to detach from the slide, but the area of interest can be underrepresented. Bones are surrounded by muscle and depending on age and species, by cartilage. Bone or cartilage need to be excluded from the analysis of the bone marrow. It is preferable not to select areas with muscle or cartilage, but in the case of cores that contain a different tissue, those areas can be discarded when the TMA is being analyzed (Fig. 9). The researcher needs to establish the minimum size of the area of interest on each core to be valid. It is recommended to use at least two or three cores per sample.

4.2.3. How to select bone marrow cores for a tissue microarray

One needs to select the type of mouse bone type to include in the TMA based on the aim of each experiment. If you want to analyze trabecular bone, sternebrae are easy to work with, as each sternebra is about the size of a 1 mm core. However, most of the image analysis studies on bone marrow have been performed on femurs, tibiae and cranium, which can also be used for TMA. Human bone marrow core biopsies are taken from the iliac crest and represent trabecular bone. It is important that a haematopathologist mark the area of interest on the H&E slides, in order to avoid subcortical biopsies, or artifacts (Fig. 10).

After core selection, the remaining tissue from the bone marrow blocks, either from mouse or human, will not be damaged. As shown in

Table 1
A comparison of tissue macroarrays and tissue microarrays.

	Tissue macroarray single specimens[a]	Tissue macroarray	Tissue microarray TMA
Limited number of specimens	X	X	X
Preservation of intact original block	X		
Area of interest > 1 mm	X	X	
Study experimental and control groups on the same slide	X	X	X
Large number of samples (hundreds)			X
Area of interest < 1 mm			X

[a] Each sample is embedded in different blocks, but after cutting, they are placed on the same slide.

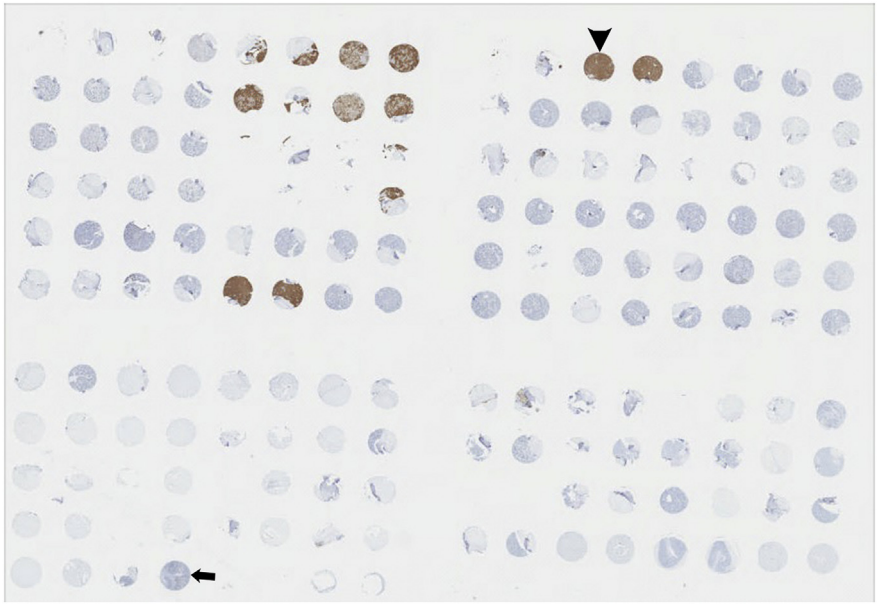

Fig. 5. An example of a tissue microarray (TMA). Photomicrograph of a TMA (4 μm sections) from mouse bone marrow samples. The design of the TMA is asymmetrical (having more rows in one direction) to control the orientation of the slide. The TMA includes a positive control (arrowhead) and negative control (arrow). The slide has been digitalized using an Aperio CS2 scanner.

Fig. 11, the core will only leave a hole in the spot that was taken, this is not different from soft tissue, as the bone marrow has been previously been decalcified.

4.2.4. Tissue microarrays for studying hematopoietic and stromal cells in human bone marrow

The use of TMA for studying the hematopoietic and stromal compartments of the bone marrow has been validated by several studies that have shown that the results found on TMAs correlated to those obtained with whole tissue sections of bone marrow trephines [52,56–59]. These findings support the proposal by Naiem et al. [60], that each bone contains a specific number of repeating structures resembling a fractal organization. Flores-Figueroa and Gratzinger have further discussed this notion. They proposed that all bone marrow elements are arranged on subunits, denominated hematopoietic units (HU) [61], which are connected by the vascularity and localized within the intratrabecular space. The composition of a HU may vary between species, type of bone and with age [61].

The interactions and composition of the stromal cells and the bone marrow microenvironment has been explored using TMA. TMA have been successfully used for the assessment of microvessel density [62] iron stores and macrophage heme oxygenase 1 expression in myelodysplastic syndromes patients [63] and the numbers of megakaryocytes, micro-vessel density and myelofibrosis in myeloproliferative neoplasms [56]. The frequency and location of CD271+ mesenchymal stromal cells in benign, dysplastic and leukemic bone marrow has been studied by TMA [64] and demonstrated that the results correlated to those with whole tissue from human bone marrow biopsies [57], where they have been validated as independent prognostic factors [53].

5. Imaging in 3 dimensions: laser scanning confocal microscopy

While 2D imaging studies provide valuable information about tissue sections, as discussed above, these studies lack depth discrimination and are not suitable to image thick or highly scattering samples, such as bone. To understand the spatial and temporal distribution of cells, the structure of the tissue must be kept intact, thus microscopy techniques are a valuable tool to interrogate the different niches that exist in the bone marrow microenvironment. One of the simplest techniques to achieve this is using basic wide-field fluorescence microscopy but there are significant limitations to this technique and the foremost of it all is

Table 2
A representative TMA map.

TMA ID:																		
TOP left								Sector 1			Sector 2							
	Row	7.0	8.2	9.4	10.6	11.8	13.0	14.2	15.4	16.6	17.8	19.0	20.2	21.4	22.6	23.8	25.0	26.2
Column		0	1	2	3	4	5	6	7	8	9	10	11	12	13	14	15	16
21.0	0	101	101	102	102	103	103	104	104	*1*	201	201	202	202	203	203	204	204
19.8	1	105	105	106	106	107	107	108	108	*2*	205	205	206	206	207	207	208	208
18.6	2	109	109	110	110	111	111	112	112	*3*	209	209	210	210	211	211	212	212
17.4	3	113	113	114	114	115	115	116	116	*4*	213	213	214	214	215	215	216	216
16.2	4	117	117	118	118	119	119	120	120	*5*	217	217	218	218	219	219	220	220
15.0	5	121	121	122	122	123	123	124	124	*6*	221	221	222	222	223	223	224	224
13.8	6	*1*	*2*	*3*	*4*	*5*	*6*	*7*	*8*		*1*	*2*	*3*	*4*	*5*	*6*	*7*	*8*
12.6	7	301	301	302	302	303	303	304	304	*1*	401	401	402	402	403	403	404	404
11.4	8	305	305	306	306	307	307	308	308	*2*	405	405	406	406	407	407	408	408
10.2	9	309	309	310	310	311	311	312	312	*3*	409	409	410	410	411	411	412	412
9.0	10	313	313	314	314	315	315	316	316	*4*	413	413	Liver	Liver	Cerebrum	Cerebrum	Kidney	Kidney
7.8	11	Heart	Heart	Spleen 2	Spleen 2	Spleen	Spleen	Lungs	Lungs	*5*								
Bottom left								Sector 3			Sector 4							

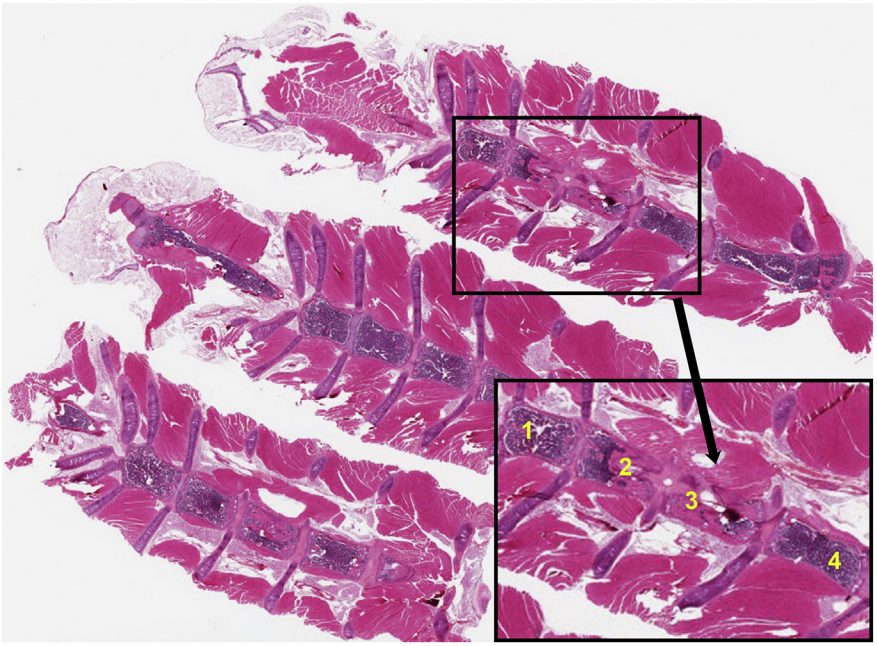

Fig. 6. Quality control of the tissue macroarray. Photomicrograph of a tissue array composed of three mouse sternums. The slide (4 μm) has been stained with H&E. The inset of one of the sternebrae shows that sternebrae 1 and 4 are intact but sternebrae 2 and 3 have muscle instead of hematopoietic tissue, caused by irregular embedding. Using a deeper cut can solve this artifact.

its limitation to 2D imaging. Considering the complexity of the bone marrow microenvironment, 2D imaging techniques are limited in visualizing and analyzing the 3D interactions between the various cell types within the bone marrow [65].

To overcome this limitation, the application of laser scanning confocal microscopy (LSCM) techniques allows us to visualize the tissue in 3D, along with other applications, such as intravital microscopy, that will be discussed further below in Section 5.2. LSCM uses lasers to excite fluorescent molecules within the sample and distinguish between different focal planes and increasing z-resolution using a small pinhole to block out-of-focus light from the detector in the imaging system (Fig. 12). This approach achieves a slicing effect that allows the visualization of proteins and structure in 3D with a high degree of spatial resolution.

There are some major limitations of confocal microscopy such as sample thickness; with increasing depth, signal intensity decreases proportionally. While this may be overcome by samples with strong fluorescence emission signal, this is often not the case for most samples. Additionally, photobleaching is a serious issue as increased sample thickness often means increased scan times which will cause photobleaching of the samples over time. In standard confocal microscopy, the excitation laser excites fluorophores along the z-axis through the full depth of the sample but images are taken for every focal plane; therefore, during the scanning process fluorophores above and below the focal plane currently being imaged are constantly excited and gradually photobleached [66].

The axial (z) resolution of the confocal microscopy is always worse than the lateral (x and y) resolution by a factor of 3. The highest lateral resolution that can be achieved using standard confocal microscopy is approximately 150 nm while axial resolution is typically at 500 nm. This means that in 3D imaging there is a discrepancy in the resolution between the lateral and axial dimensions.

Another limitation of the technique is inherent in the fluorophores most commonly used for live cell imaging, which excite at around

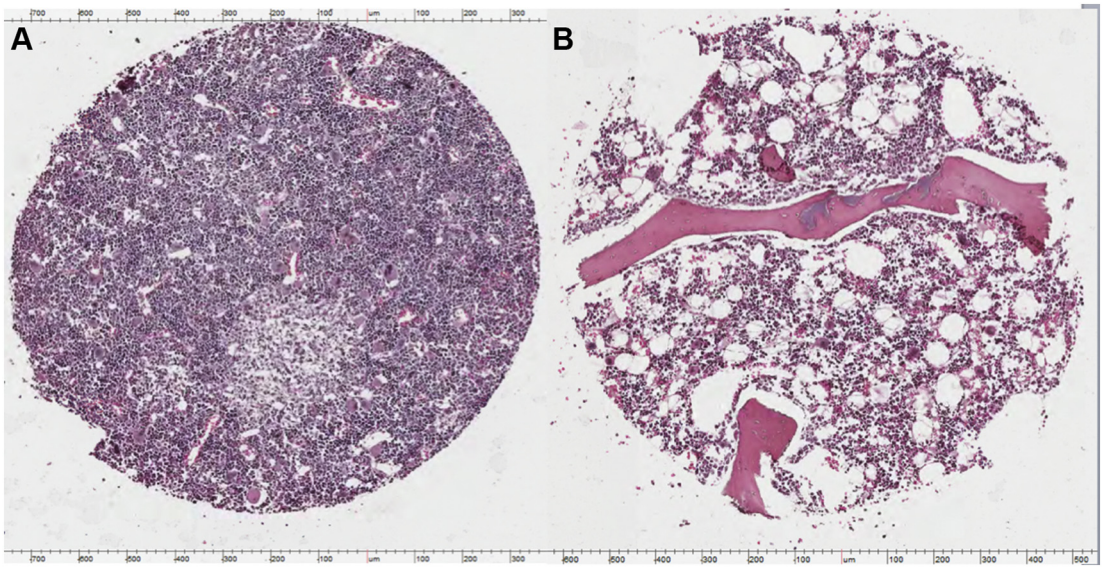

Fig. 7. Representative bone marrow TMA cores. Photomicrographs of two H&E stained human bone marrow cores. A) 1 mm core from a human bone marrow biopsy with 100% cellularity. B) 1 mm core from a human bone marrow biopsy with 60% cellularity.

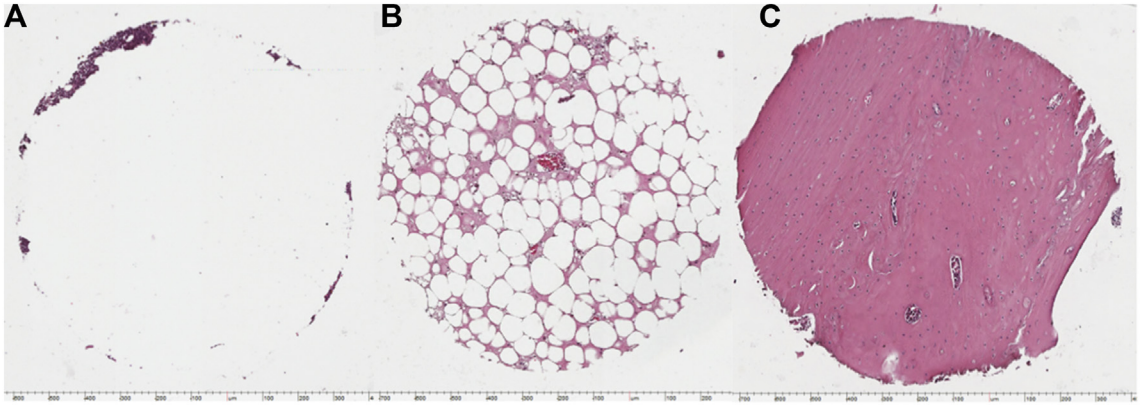

Fig. 8. Bone marrow TMA cores that cannot be used for studies. Photomicrographs of three H&E stained human bone marrow cores. A) Empty or missing spot. B) Human bone marrow core with < 10% of cellularity, the core is filled with adipocytes. C) Core with muscle and not hematopoietic tissue.

400–500 nm wavelengths. At these wavelengths, which are close to the ultraviolet range, the laser could induce phototoxicity in the samples during the imaging process. More advanced approaches have been developed to overcome some of the limitations present in basic confocal microscopy: on one side, far red shifted fluorophores are increasingly utilized (see above), on the other side, multiphoton microscopy allows exploiting less phototoxic infrared wavelength for fluorophore excitation.

LSCM acquires a series of optical sections, by rejecting the light from out-of-focus z planes, and is therefore ideal for thick specimens. It has been often used for imaging tissue sections and for intravital microscopy (IVM), which is discussed further below. Nevertheless, LSCM is limited to the tissue surface and for depths over 100 μm there is increased light scattering, which limits the contrast and signal strength. Despite this, LSCM has become an increasingly popular tool to study interactions of HSCs with their niche cells.

Traditional methods for the study of hematopoietic stem and progenitor cell (HSPC) niches in the bone marrow in vivo involved the transplantation of FACS sorted genetically or chemically labelled HSPCs [67] into recipient mice and studying the homing of transplanted HSPCs in the recipient mice BM. The limitation of this study is the fact that functional, engrafting HSPCs were observed only within the myeloablated recipient mice, however the myeloablation achieved through irradiation causes alterations to the BM niche cells such as endothelial cells [68], osteoblasts [69] and bone itself [44], preventing the study of native HSPCs and their niche in unperturbed environments. The development of the SLAM markers, which allowed for the identification of HSPCs using a limited panel of markers, allowed for the first analysis of HSPCs in native BM sections imaged using LSCM [70]. It has since been recognized that SLAM HSPCs are heterogeneous and require further purification (and hence more than four colors) to separate HSCs from multipotent progenitors [71,72], nevertheless, this was a key study that was a significant step forward in increasing the popularity of histological studies of HSPCs in BM sections.

In the last decade, there have been numerous studies using LSCM technology together with a combination of reporter mice and antibodies to study HSC niches. All of these studies have advanced our understanding of the HSC niche, but have also contributed further to the controversy about the nature of HSC niches. These studies are revealing that there are numerous different niche cell types that contribute to the regulation of HSCs, and that quiescent and cycling HSCs have different niches [10,12,73]. The recent reviews by Gao et al. [4] and Crane et al. [3] have provided excellent overviews of these studies, hence they are not discussed further here.

5.1. Multiphoton microscopy

Despite the advances that LSCM studies have provided in studies of HSC niche, to fully capture all the interactions of the HSC with the surrounding microenvironment cells, 3D analysis in thick tissues are required; alternatively, serial sections can be used as a substitute but it increases the complexity and labor required. Additionally, the BM is a highly dynamic environment and a single time point is not sufficient to capture the dynamic interactions, nor does it let the investigator know if the cell is truly in its niche, or if it is just passing through the bone marrow in that particular location at that given time.

To overcome the limitations of sample thickness and phototoxicity, a technique known as two-photon excitation fluorescence (TPEF) microscopy is utilized [74,75]. TPEF is achieved through the excitation of a fluorophore by two photons of double the wavelength (thus half the energy) required to excite the molecule; thus using infra-red lasers (i.e. 800 nm) to excite fluorophores in the UV range (i.e. 400 nm). When the

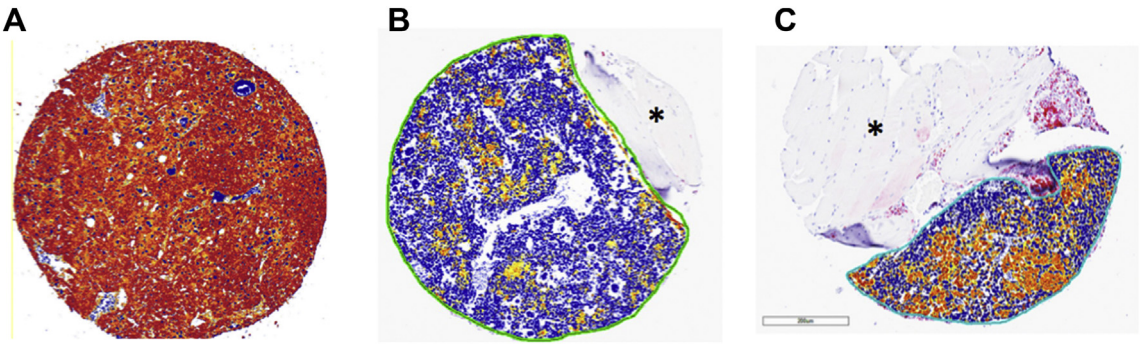

Fig. 9. Image analysis of bone marrow cores. Core A has no muscle or bone, cores B and C have muscle (asterisk) that has been eliminated in the image analysis. Positive signal (red, orange and yellow). Negative stain (blue). (For interpretation of the references to color in this figure legend, the reader is referred to the web version of this article.)

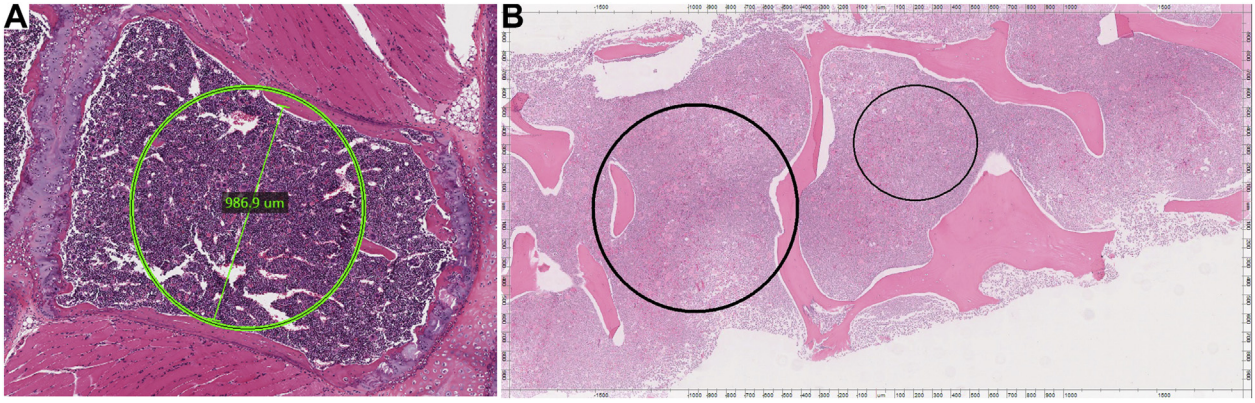

Fig. 10. Selection of bone marrow cores. Photomicrograph of A) a mouse sternebra and B) a human bone marrow biopsy. The circles represent the area of a core. In the human bone marrow biopsy two different areas have been selected a 0.6 mm core (smaller circle) and a 1 mm core (largest circle). Each area is placed on the parenchyma of the bone marrow.

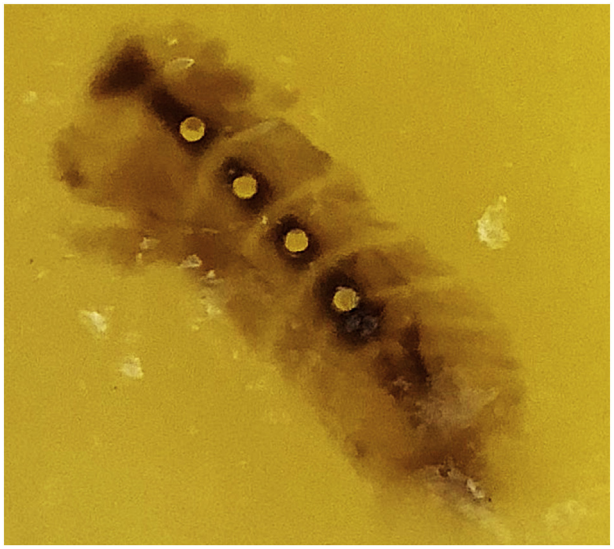

Fig. 11. A photograph from a mouse sternum, where four cores of 0.6 mm have been taken. The remaining tissue is intact.

two photons excite the fluorophore at extremely close intervals (femtoseconds), it will cause the energy from both photons to combine and excite the fluorophore as if it is excited by a single fluorophore containing the combined energy of the two photons. This is achievable through the utilization of a femto-second (fs) pulsed laser to deliver extremely short pulses of photons onto the sample at high repetition rates [76]. Additionally, the excitation laser in a TPEF system is focused onto the focal plane and excitation does not happen above or below the focal plane (out of focus region) thus eliminating the need for a pinhole. This focused excitation has the benefit of increasing resolution, especially in deeper samples and tissues characterized by high scattering such as the bone marrow (Fig. 13), and of reducing photodamage as fluorophores in the out of focus plane are not excited during the acquisition process [76].

3D imaging of thick tissue sections can be better achieved by using multiphoton microscopy (MP) [77]. MP includes any microscopy that uses at or above 2-photon microscopy, and has the capability to image thicker pieces of tissues; with depths ranging from 150 μm, such as in the calvarium [78] to 500 μm deep in soft tissues like the lymph nodes [79]. The advantages of MP microscopy stems from its use of near infrared light (700–1000 nm) to excite the fluorophores, the higher the wavelength of the excitation laser, the greater the penetration ability thus allowing excitation deeper into the tissue. In addition, infra-red light has less phototoxicity and photobleaching, in comparison to the UV and visible light lasers used in LSCM [76]. 2-Photon excitation also allows better 3D resolution, photolytic release of caged molecules and second harmonic generation (SHG) signal to image the collagen 1 fibres that compose the bone itself [80–82]. These strategies are often used in isolation, however, the combination of reporter mice, antibodies and SHG signals allows for the simultaneous imaging of different BM niche cell components either in sections or in live imaging as recently shown by Duarte et al. [49].

In summary, the major advantages of this technique are the increase in sample penetration (of up to 1 mm in thickness in the case of brain) and reduced phototoxicity. This is due to the use of infra-red lasers which have far higher sample penetration than lasers of lower wavelengths, and lower phototoxicity as fluorophores are no longer excited with lasers close to the UV range [76].

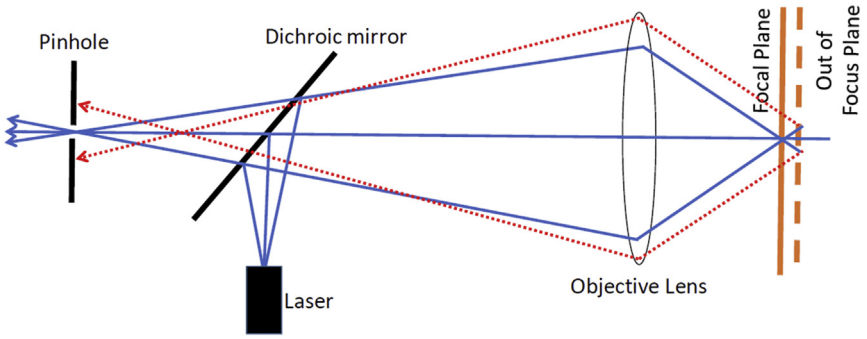

Fig. 12. Schematic of basic confocal microscopy. The pinhole blocks out of focus light (red dotted line) originating from the out of focus plane while allowing in focus light (blue line) to pass to the detector. (For interpretation of the references to color in this figure legend, the reader is referred to the web version of this article.)

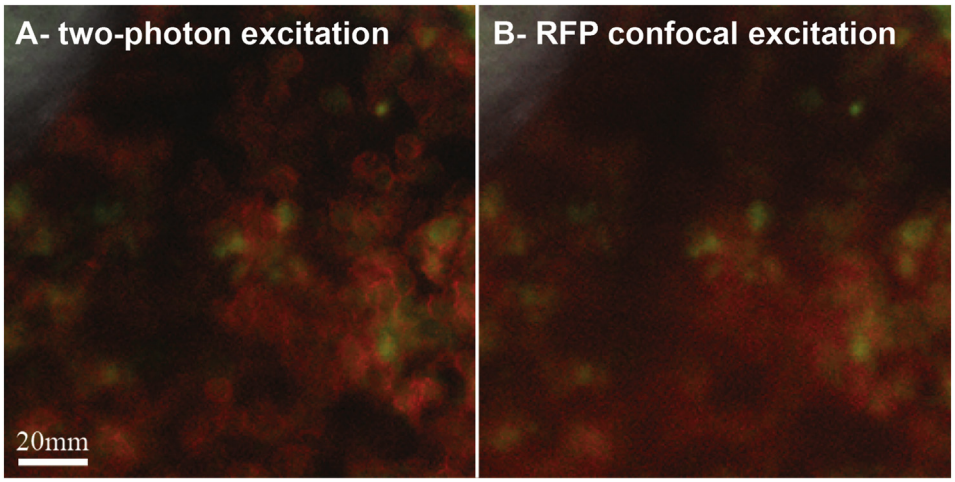

Fig. 13. Two-photon excitation of deep bone marrow. Two-photon excitation increases spatial resolution. A 2D image of the same deep BM area containing H2BGFP + mTmG + hematopoietic cells was acquired (A) using 970 nm and 1030 nm two-photon excitation, and (B) using 970 nm two photon and 561 nm confocal excitation. Red: membrane tomato; green: GFP; grey: bone collagen SHG. (For interpretation of the references to color in this figure legend, the reader is referred to the web version of this article.)

5.2. Intravital microscopy

Due to their ability to excite fluorescence in thick tissues, LSCM and particularly MP microscopy, have been used in time-lapse mode either alone or in combination to perform IVM and capture biological processes in four dimensions (4D). IVM permits real-time imaging of cell-cell interactions and cell differentiation in BM niches, capturing the dynamics and complexities of biological processes that are not possible to detect in static tissue sections. Processes that can be captured using IVM include, for example, information of a cell's motility, and, if a cell is determined to be mobile, how fast it is moving and where is it moving to; the interactions of distinct cells with other cell types; the time taken for a cell to divide, and the ability to detect other cellular properties in living cells in real time, such as apoptosis [83–85].

The limitations of IVM studies are that the ability to detect different niche cell types and HSCs require methods that permit the detection of these cells in living animals. Numerous reporter mice are routinely used; however, these mice also have limitations (see above). Fortunately, many fluorophore-conjugated antibodies and reagents can be intravenously injected into the live mouse to visualize different bone marrow niche cell types when performing IVM. For example, methods for detecting endothelial cells include the use of Dil-labelled acetylated low-density lipoprotein (Dil-Ac-LDL) [73], fluorescently conjugated *Griffonia simplicifolia* isolectin B4 (IB4) [86] or fluorophore-conjugated antibodies specific for endothelial antigens [87]. It should be noted, however, that macrophages, which are abundant in bone marrow, readily take up Ac-LDL [88] and IB4 has also been shown to be an excellent marker of macrophages [89]. Blood vessels are also often identified in IVM studies using intravascular dyes, such as fluorescently tagged bovine serum albumin (BSA), dextrans with various molecular weights (note that, again, particularly high molecular weight dextrans should be used to minimize extravasation from bone marrow sinusoids and macrophage labelling), and non-targeted Quantum dots (Qdots) have also been successfully used for IVM studies [78]. Using this approach, human leukemic cells have been visualized in the bone marrow [18], and immune cells in multiple tissues [90].

For studies assessing HSC niches in bones, the best results are obtained using bones that are readily accessible. Some initial studies, such as those by Xie et al. [91] transplanted mice with phenotypic HSCs then removed the tibiae and femurs of the mice and imaged them outside of the body, using a method called ex vivo imaging of stem cells (EVISC). This study suggested that after irradiation the endosteal area becomes highly stimulatory, promoting HSC expansion. It is important to note, however, that the imaging was performed using bones that had been removed from the mouse, and hence lacked the innervation from nerves and blood vessels, which have been shown to be important in regulating HSCs [92].

Furthermore, while other investigators have since modified methods to use long bones in IVM imaging studies, these studies require significant manipulation of the thick bone to be able to image the bone marrow. Some studies, such as those by Köhler et al., who revealed differential positioning and activity of young and aged HSCs [93], and Pitt et al., who studied the interactions between T-cell acute lymphoblastic leukemia (T-ALL) cells and CXCL12-producing stromal cells in the BM [94], thinned the bone (using methods such as shaving the bone) prior to imaging. The impact of this bone thinning on the overall function of the bone microenvironment is unclear, however, osteocytes, which are embedded within the bone matrix, are known to communicate with cells within the bone marrow and have been implicated in regulating the mobilization of HSCs [95].

In a different approach, Lewandowski et al. used a fiber-optic imaging system akin to a miniaturized endoscope and inserted it directly into the femoral bone cavity via the knee to image the central marrow [96]. Although highly invasive and disruptive for the tissue, this approach allowed imaging of the interactions of HSCs and endothelial cells in central bone marrow, and revealed an important role for reactive oxygen species in the regeneration of bone marrow after a bone marrow transplant. The question remains whether some of the interactions were the result of cell compaction in front of the advancing probe.

In contrast to the challenges of imaging bone marrow in long bone, the calvarium (skull bone) is very thin and does not require manipulation (such as shaving) prior to imaging. It is also less invasive to readily access this skull bone repeatedly in living mice, and is covered by a thin skin that can readily be removed to expose the bone surface for imaging. Importantly, the calvarium has been shown to be as representative as the femur and the tibia in the study of hematopoiesis in mice [78,86]. The von Andrian group pioneered studies of calvarium BM, using epifluorescence microscopy to study HSPC rolling in vessels [97]. More recently, laser-mediated osteotomy of the calvarium has been used to improve the quality of the imaging studies [98].

In the first IVM studies of HSC niches in calvarium BM, Lo Celso et al. showed that LT-HSCs localize very closely to endosteal Col 2.3GFP + osteoblasts in irradiated recipients and to the endosteum in both irradiated wildtype mice and in non-irradiated W/Wv mice, the latter which permit engraftment without requiring prior irradiation [78]. In contrast, the more mature progeny of LT-HSCs were found to be distal from the endosteal osteoblasts [78]. A refined technology from the Lo Celso lab resulted in the ability to repeatedly image the same area of calvarium BM over very long periods of time, hours (Fig. 14) or days apart [18]. This technology allowed the mouse to be either imaged over the course of a number of hours, or to be removed from the imaging platform in between imaging sessions, with the exact same region imaged longitudinally in subsequent imaging sessions [85]. This

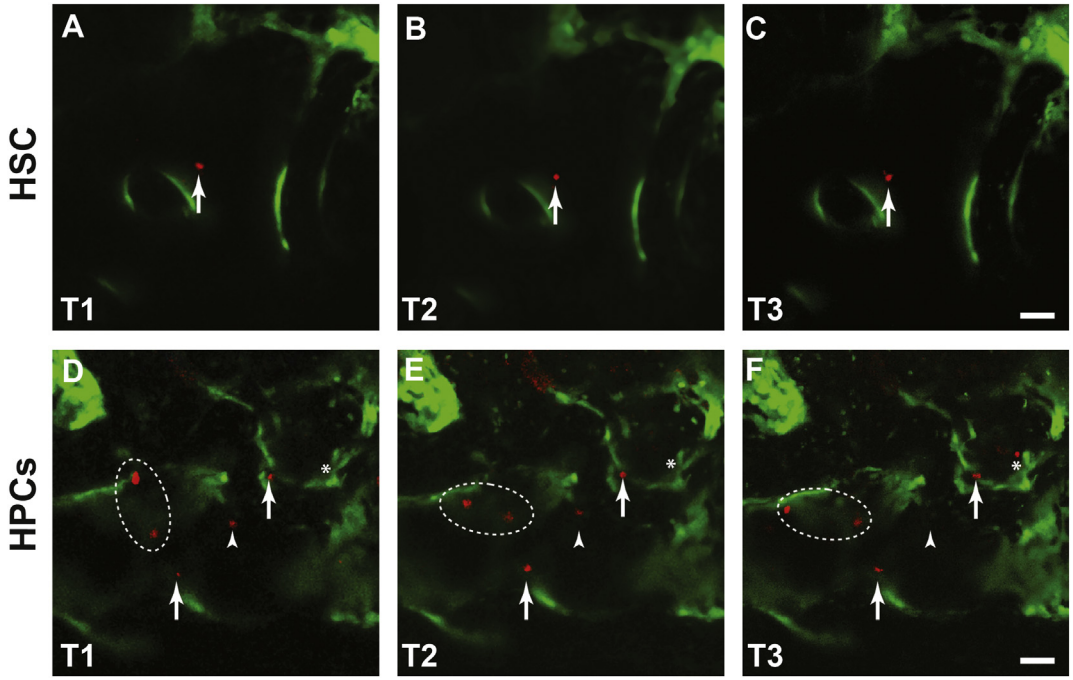

Fig. 14. Longitudinal IVM of mouse bone marrow. DiD labelled HSCs (A–C) or hematopoietic progenitor cells (HPC) (D–F) were injected into a col2.3GFP mouse and imaged three times within the same day [T1 = 0′, T2 = 150′ and T3 = 330′ (C) / 390′ (F)]. Green: osteoblastic cells, red: DiD labelled cells. Arrows point at static cells, arrowhead at a cell that disappears, asterisk highlights an area where an HPC appears during the last session, dotted line encircles two cells that may move. Scale bars: 50 μm. (For interpretation of the references to color in this figure legend, the reader is referred to the web version of this article.)

adaptation has permitted the study of the interactions between LT-HSCs and osteoblasts and between leukemia cells and multiple components of the bone marrow microenvironment over a long period of time [18,49].

To date, the studies performed using this technological platform have revealed that in the steady state, LT-HSCs are stationary and are primarily localized near osteoblasts [84]. In contrast, in response to infection, the interactions between the LT-HSCs and osteoblasts are altered, with the LT-HSCs being more motile and engaging with larger BM niches [84]. Furthermore, this platform has also been used to show that T-ALL cells destroy osteoblasts via inducing their apoptosis [18], whereas AML cells selectively remodel endosteal vessels in mice [49]. The findings of these latter two studies were validated in human studies using trephine BM sections of T-ALL [18] and AML patients [49], respectively.

The Bonnet lab has also used IVM to image human HSCs in xenotransplanted mice. In these studies, human HSCs were reported to be transiently migratory until they reached their niche, whereas more mature human hematopoietic progenitors remained motile after homing to the BM [99]. IVM studies have also been used in a mouse model of myeloma to show that osteoblasts regulate the dormancy of myeloma cells at the endosteal niche, and that osteoclasts awaken the myeloma cells from quiescence [100].

5.3. Large 3D images

As well as longitudinal, or time-lapse, imaging over extended periods of times, another type of imaging is becoming increasingly important in the hematopoietic field: this is the acquisition of images covering large areas of bone marrow, and ideally entire bone marrow cavities. Tilescan imaging is well established for the study of sections, but it is now increasingly used for intravital (Fig. 15) and whole mount images of hematopoietic tissues. Calvarium bone marrow can now be acquired in less than an hour thanks to fast acquisition protocols [18,49], and large 3D images of whole mount thick sections or cleared entire bones have been increasingly used to investigate the position of hematopoietic stem cells [73,101].

As previously mentioned, for 3D imaging the axial (z) resolution in imaging is always worse than the lateral (x and y) resolution. This issue is even more apparent when acquiring large 3D images of whole mount preparations and thick sections, where both the axial resolution and the depth of tissue that can be imaged are limited. This limitation is caused by scattering and spherical aberration of light as it passes through different components of the tissue with varying refractive indexes, with the surrounding bone itself being a major contributor to scattering and loss of signal [102]. One of the methods used to overcome this is through optical clearing techniques. The goal of optical clearing is to minimize the refractive index mismatch between the low refractive index of aqueous components of the tissue and the higher refractive index of the cell membranes and extracellular matrix (i.e. collagen) found within the same tissue. It should be noted that the tissue components (i.e. cells and extracellular matrix) vary between different tissue types and thus clearing protocols should be optimized for each tissue. Moreover, certain clearing protocols may be detrimental to the target epitope and/or the structure of the tissue. Richardson et al. provides a comprehensive review and comparison of different tissue optical clearing methods [102]. Furthermore, Acar et al. has compared the effects of various different optical clearing agents for the purpose of imaging bone marrow samples using confocal microscopy [101]. Clearing methods continue to be developed [103] and evaluated and each researcher should carefully troubleshoot this step, to avoid generation of any artefacts.

A first challenge of these types of images comes from their size, which requires appropriate computing power to be imaged and analyzed. Furthermore, complex spatial statistics need to be used to interpret the results obtained, especially measurements of relative positions relative to multiple tissue components and cell types. The distribution of two different cell types can be compared [73], or, in the absence of a comparable control population, artificial cells randomly positioned within the 3D image can be used [18]. Cytometry software has been developed to tackle these challenges [103,104], and the generation of reliable, user friendly analysis pipelines will be key to fully take advantage of the wealth of information contained in large 3D

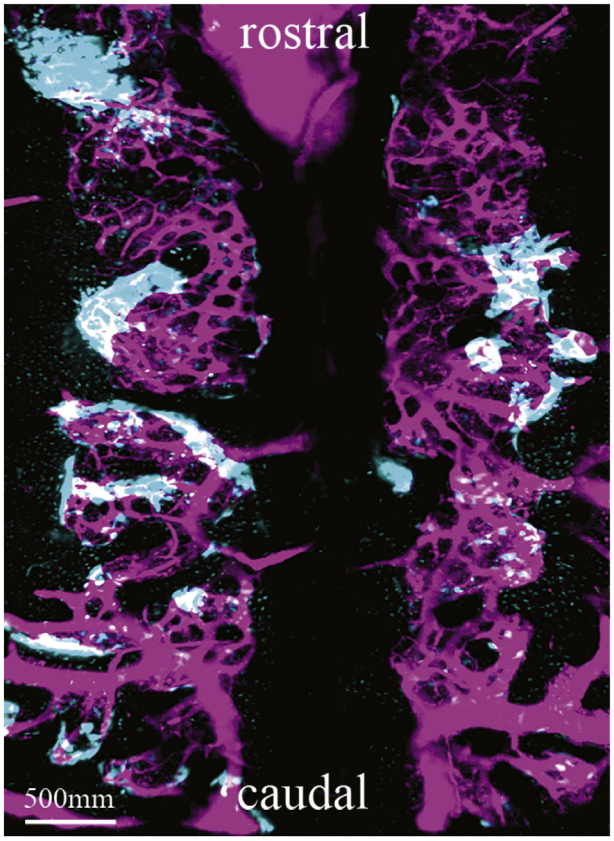

Fig. 15. Tissue-wide bone marrow microscopy. Maximum intensity projection of a 3D tilescan of mouse calvarium bone marrow. Blood vessels were identified with high molecular weight cy-5 dextran injected intravenously (magenta). Col2.3 cyan osteoblasts are shown in cyan. (For interpretation of the references to color in this figure legend, the reader is referred to the web version of this article.)

images. Big data analytical approaches, such as dimensional reduction techniques and deep learning applied to both large 3D and longitudinal images hold the promise to unravel the spatial organization of hematopoietic tissues and to solve multiple controversies still ongoing on the nature of the cellular interactions supporting hematopoiesis.

6. Emerging technologies that are advancing imaging studies of tissue sections

6.1. Spectral imaging and linear unmixing for fluorescence multiplexing

As previously mentioned, one of the limitations of fluorescence multiplexing is the spillover when multiple fluorophores with overlapping emissions are used in the same panel. Linear unmixing is a technique used to separate overlapping fluorophores by distinguishing the "spectral fingerprint" of each fluorophore. Every fluorophore has its own distinct spectral emission profile, it emits maximally at different wavelengths and the shape of the emission profile is unique to each fluorophore. Both fluorescence compensation and linear unmixing assumes that when two fluorophores have overlapping emission profiles, the combined fluorescence intensity signal for the overlapping wavelengths are the sum of the intensity from each individual fluorophore. Where fluorescence compensation "subtracts" the estimated spillover fluorescence signal to correct for the intensity of each fluorophore in each detector [33], linear unmixing uses an algorithm to calculate the contribution of each fluorophore on the combined fluorescence spectra using the known fluorescent profiles of each fluorophore as reference. Thus, theoretically, as long as the "spectral fingerprint" of each fluorophore is distinct from each other, multiple fluorophores with overlapping profiles can be used together. In practice, the greater the difference the more accurate the separation of the fluorophores using linear unmixing. It is also important that each of the fluorophores are of similar intensity as it is possible to overwhelm the signal from the weaker fluorophore when there are extreme differences in fluorescence intensities between the fluorophores. It should be noted that linear unmixing can also be set up to include autofluorescence as another fluorophore, thereby negating autofluorescence and possibly even using the inherent autofluorescence to the advantage of the researcher.

This technique has excellent synergy with the TSA method of fluorescence multiplexing. As TSA allows for the labelling of tissue sections with multiple fluorophores regardless of antibody species with ease and linear unmixing allows for the identification of multiple overlapping fluorophores.

Linear unmixing is limited by the hardware available for the acquisition of spectral images. Most of the fluorophores used in cell biology emit in the visible light range between 400 and 700 nm and the hardware have been designed for such. With spectral detectors now capable of detecting further into the infra-red region (> 700 nm) combined with fluorophore-conjugated tyramide simplifying the multiplexing protocol, it is possible to expand the utility of linear unmixing to include even more fluorophores than what is currently available.

Commercially available kits include the Opal™ multiplexing technology from Perkin Elmer, which currently permit up to 7 colors plus DAPI to be visualized on the same section [105]. Sections can be scanned using specialized imaging technology such as the Perkin Elmer Mantra, Vectra or Polaris systems; however, the technology can also be imaged using LSCMs equipped with spectral imaging and unmixing capabilities (Fig. 16).

6.2. Imaging Mass Cytometry (IMC)

The field of hematopoiesis has advanced to the point that requires robust imaging techniques to visualize complex hematopoietic subpopulations and to study the interactions between different and several subpopulations within the bone marrow. As discussed above, a significant challenge for imaging studies are the number of parameters than we can assess simultaneously. Imaging Mass Cytometry (IMC) is another novel technique based on the use of metal-tagged reagents that allows for the simultaneous imaging of at least 40 different parameters including antibodies, DNA, and mRNA. IMC is a robust technique than can be used with cytospins, frozen and paraffin embedded tissue sections [106,107]. It will enable us to study the "topobiology" [61] of benign and malignant hematopoiesis, allowing the location of single cell populations and the study of their interactions within the bone marrow.

The staining technique for IMC is similar to that used for immunofluorescence studies. It requires an antigen retrieval step (prior deparaffinization is required only if using paraffin embedded tissues), a blocking step (usually with serum) and staining procedure. Tissue sections or cell slides, including cytospins [108] are incubated with a mixture of metal-tagged antibodies. This technique can be multiplexed to detect both proteins and mRNA [109,110]. The largest limitation of this technology is that the slide cannot be visualized under a fluorescent microscope, but needs to be ablated with a laser and analyzed with a mass cytometer [Hyperion™ Imaging System (Fluidigm, Inc.)] which is able to detect dozens of parameters simultaneously with subcellular resolution [108]. Finally the image is reconstructed digitally [106,107] (Fig. 17).

7. Conclusions

During the last decade there have been significant advances in our ability to image HSCs and HSC niches in tissues and living animals, providing investigators with a range of techniques with which to study

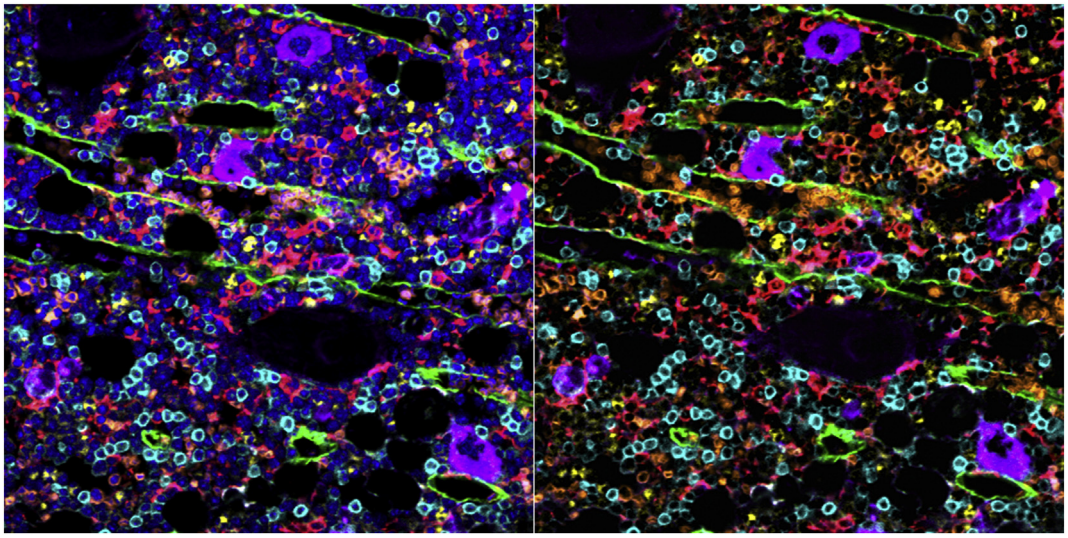

Fig. 16. Multiplexing with 7 colors on a single BM section. The Opal™ kit commercially available from Perkin Elmer consists of 6 fluorophores with distinct spectral emission profiles that uses the TSA technique for signal amplification, combining the advantages of both TSA and linear unmixing together to achieve robust multispectral imaging of up to 7 colors in tissue (6 fluorophores + DAPI for nuclei). Shown is a BM section from a paraformaldehyde fixed, paraffin-embedded mouse tibia that was stained with antibodies against BM sinusoids and different maturing hematopoietic cells, allowing ease of identification of all colors separately on the same section using the Opal™ kit. Both panels show the same image, however, DAPI has been excluded from the right panel. These images were scanned and acquired on a Nikon A1R LSCM. Yellow (Opal 540) = Gr-1 + granulocytes, orange (Opal 570) = Ter119 + erythrocytes, red (Opal 620) = F4/80 + macrophages, purple (Opal 650) = vWF + megakaryocytes, cyan (Opal 690) = B220 + B lymphocytes and green (Opal 520) = vascular endothelial growth factor-3 (VEGFR-3) + BM sinusoids, plus blue (DAPI) nuclear stain. (For interpretation of the references to color in this figure legend, the reader is referred to the web version of this article.)

interactions of HSCs and their niches in normal and diseased states. The recent development of multiplexing technologies will permit the detection of numerous rare cells in the same tissue in a manner that has never been possible before, and will significantly aid the study of human HSC niches in bone marrow biopsies. Finally, while this review has focused on HSC niches, the technologies overviewed here are applicable to the studies of numerous different tissues in normal and diseased states, and will likewise significantly contribute to advances in numerous research fields.

Acknowledgements

We thank Olga Ornatsky for her helpful comments and edits on Imaging Mass Cytometry, and Fluidigm for supplying the images shown for Imaging Mass Cytometry. This review was supported in part by grants from the European Research Council (ERC STG 337066), the British Biology and Biotechnology Research council (BB/i004033/1) and Bloodwise (12033 and 15040) to CLC, the National Health and Medical Research Council of Australia grant 1127551 to LEP and the Victorian State Government Operational Infrastructure Support Program (to St. Vincent's Institute). EFF was supported by the “Sectorial Fund for Research in Health and Social Care” (Fondo Sectorial de Investigación en Salud y Seguridad Social) grant number: Conacyt (272793), the “Research Fund for Frontiers in Science” (Fondo de Investigación en Fronteras de la Ciencia) grant number: Conacyt 2015-2 (FC-2015-2/1341), International cooperation program (IMSS) and the

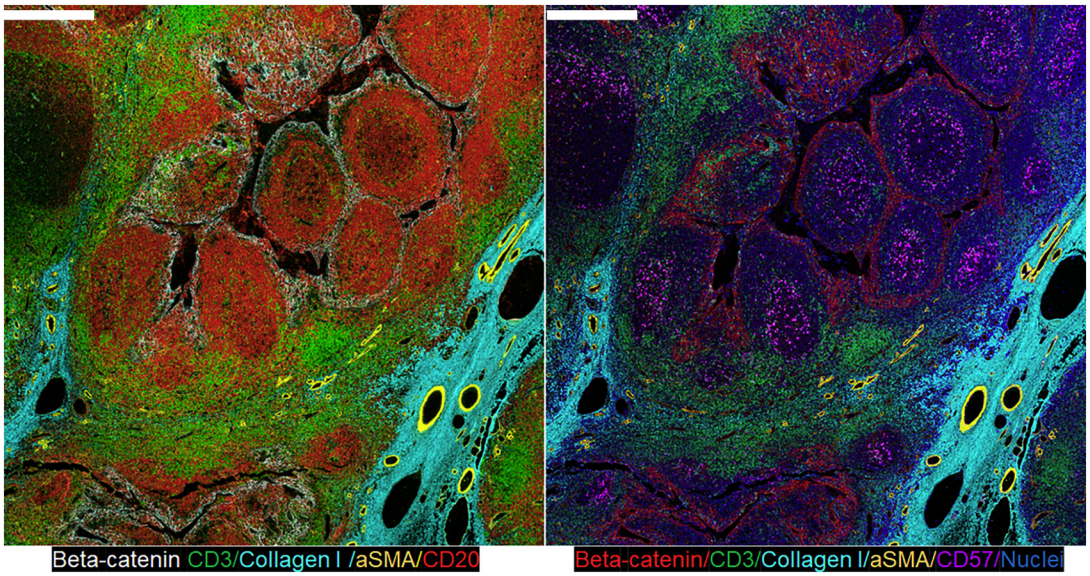

Fig. 17. Multiplexing using image mass cytometry. Images of formalin fixed, paraffin-embedded human tonsil sections that have been stained with 5 different markers plus nuclear stain (right panel) as described. The scale bars represent 500 µm.

Canada-Israel Health Research Initiative, jointly funded by the Canadian Institutes of Health Research, the Israel Science Foundation, the International Development Research Centre, Canada and the Azrieli Foundation. DD was supported by the FCT fellowship SFRH/BD/52195/2013.

References

[1] S.J. Morrison, D.T. Scadden, The bone marrow niche for haematopoietic stem cells, Nature 505 (7483) (2014) 327–334.
[2] L.E. Purton, D.T. Scadden, The hematopoietic stem cell niche, StemBook, 2008 (Cambridge (MA)).
[3] G.M. Crane, E. Jeffery, S.J. Morrison, Adult haematopoietic stem cell niches, Nat. Rev. Immunol. 17 (9) (2017) 573–590.
[4] X. Gao, C. Xu, N. Asada, P.S. Frenette, The hematopoietic stem cell niche: from embryo to adult, Development 145 (2) (2018).
[5] M. Askmyr, N.A. Sims, T.J. Martin, L.E. Purton, What is the true nature of the osteoblastic hematopoietic stem cell niche? Trends Endocrinol. Metab. 20 (6) (2009) 303–309.
[6] J. Isern, A. Garcia-Garcia, A.M. Martin, L. Arranz, D. Martin-Perez, C. Torroja, F. Sanchez-Cabo, S. Mendez-Ferrer, The neural crest is a source of mesenchymal stem cells with specialized hematopoietic stem cell niche function, elife 3 (2014) e03696.
[7] A. Greenbaum, Y.M. Hsu, R.B. Day, L.G. Schuettpelz, M.J. Christopher, J.N. Borgerding, T. Nagasawa, D.C. Link, CXCL12 in early mesenchymal progenitors is required for haematopoietic stem-cell maintenance, Nature 495 (7440) (2013) 227–230.
[8] L. Ding, S.J. Morrison, Haematopoietic stem cells and early lymphoid progenitors occupy distinct bone marrow niches, Nature 495 (7440) (2013) 231–235.
[9] B.O. Zhou, R. Yue, M.M. Murphy, J.G. Peyer, S.J. Morrison, Leptin-receptor-expressing mesenchymal stromal cells represent the main source of bone formed by adult bone marrow, Cell Stem Cell 15 (2) (2014) 154–168.
[10] T. Itkin, S. Gur-Cohen, J.A. Spencer, A. Schajnovitz, S.K. Ramasamy, A.P. Kusumbe, G. Ledergor, Y. Jung, I. Milo, M.G. Poulos, A. Kalinkovich, A. Ludin, O. Kollet, G. Shakhar, J.M. Butler, S. Rafii, R.H. Adams, D.T. Scadden, C.P. Lin, T. Lapidot, Distinct bone marrow blood vessels differentially regulate haematopoiesis, Nature 532 (7599) (2016) 323–328.
[11] Y. Omatsu, T. Sugiyama, H. Kohara, G. Kondoh, N. Fujii, K. Kohno, T. Nagasawa, The essential functions of adipo-osteogenic progenitors as the hematopoietic stem and progenitor cell niche, Immunity 33 (3) (2010) 387–399.
[12] A.P. Kusumbe, S.K. Ramasamy, T. Itkin, M.A. Mae, U.H. Langen, C. Betsholtz, T. Lapidot, R.H. Adams, Age-dependent modulation of vascular niches for haematopoietic stem cells, Nature 532 (7599) (2016) 380–384.
[13] C. Joseph, J.M. Quach, C.R. Walkley, S.W. Lane, C. Lo Celso, L.E. Purton, Deciphering hematopoietic stem cells in their niches: a critical appraisal of genetic models, lineage tracing, and imaging strategies, Cell Stem Cell 13 (5) (2013) 520–533.
[14] A.C. Green, V. Rudolph-Stringer, A.D. Chantry, J.Y. Wu, L.E. Purton, Mesenchymal lineage cells and their importance in B lymphocyte niches, Bone (2017).
[15] Z. Kalajzic, P. Liu, I. Kalajzic, Z. Du, A. Braut, M. Mina, E. Canalis, D.W. Rowe, Directing the expression of a green fluorescent protein transgene in differentiated osteoblasts: comparison between rat type I collagen and rat osteocalcin promoters, Bone 31 (6) (2002) 654–660.
[16] S. Mendez-Ferrer, T.V. Michurina, F. Ferraro, A.R. Mazloom, B.D. Macarthur, S.A. Lira, D.T. Scadden, A. Ma'ayan, G.N. Enikolopov, P.S. Frenette, Mesenchymal and haematopoietic stem cells form a unique bone marrow niche, Nature 466 (7308) (2010) 829–834.
[17] S.J. Rodda, A.P. McMahon, Distinct roles for Hedgehog and canonical Wnt signaling in specification, differentiation and maintenance of osteoblast progenitors, Development 133 (16) (2006) 3231–3244.
[18] E.D. Hawkins, D. Duarte, O. Akinduro, R.A. Khorshed, D. Passaro, M. Nowicka, L. Straszkowski, M.K. Scott, S. Rothery, N. Ruivo, K. Foster, M. Waibel, R.W. Johnstone, S.J. Harrison, D.A. Westerman, H. Quach, J. Gribben, M.D. Robinson, L.E. Purton, D. Bonnet, C. Lo Celso, T-cell acute leukaemia exhibits dynamic interactions with bone marrow microenvironments, Nature 538 (7626) (2016) 518–522.
[19] Y. Xu, L. Yuan, J. Mak, L. Pardanaud, M. Caunt, I. Kasman, B. Larrivée, R. del Toro, S. Suchting, A. Medvinsky, J. Silva, J. Yang, J.-L. Thomas, A.W. Koch, K. Alitalo, A. Eichmann, A. Bagri, Neuropilin-2 mediates VEGF-C–induced lymphatic sprouting together with VEGFR3, J. Cell Biol. 188 (1) (2010) 115.
[20] O. Shimomura, F.H. Johnson, Y. Saiga, Extraction, purification and properties of aequorin, a bioluminescent protein from the luminous hydromedusan, Aequorea, J. Cell. Comp. Physiol. 59 (1962) 223–239.
[21] R.N. Day, M.W. Davidson, The fluorescent protein palette: tools for cellular imaging, Chem. Soc. Rev. 38 (10) (2009) 2887–2921.
[22] M.V. Matz, A.F. Fradkov, Y.A. Labas, A.P. Savitsky, A.G. Zaraisky, M.L. Markelov, S.A. Lukyanov, Fluorescent proteins from nonbioluminescent Anthozoa species, Nat. Biotechnol. 17 (10) (1999) 969–973.
[23] N.C. Shaner, R.E. Campbell, P.A. Steinbach, B.N. Giepmans, A.E. Palmer, R.Y. Tsien, Improved monomeric red, orange and yellow fluorescent proteins derived from *Discosoma* sp. red fluorescent protein, Nat. Biotechnol. 22 (12) (2004) 1567–1572.
[24] D.M. Chudakov, M.V. Matz, S. Lukyanov, K.A. Lukyanov, Fluorescent proteins and their applications in imaging living cells and tissues, Physiol. Rev. 90 (3) (2010) 1103–1163.
[25] H.J. Snippert, L.G. van der Flier, T. Sato, J.H. van Es, M. van den Born, C. Kroon-Veenboer, N. Barker, A.M. Klein, J. van Rheenen, B.D. Simons, H. Clevers, Intestinal crypt homeostasis results from neutral competition between symmetrically dividing Lgr5 stem cells, Cell 143 (1) (2010) 134–144.
[26] V.W.C. Yu, R.Z. Yusuf, T. Oki, J. Wu, B. Saez, X. Wang, C. Cook, N. Baryawno, M.J. Ziller, E. Lee, H. Gu, A. Meissner, C.P. Lin, P.V. Kharchenko, D.T. Scadden, Epigenetic memory underlies cell-autonomous heterogeneous behavior of hematopoietic stem cells, Cell 168 (5) (2017) 944–945.
[27] H. Ueno, I.L. Weissman, Clonal analysis of mouse development reveals a polyclonal origin for yolk sac blood islands, Dev. Cell 11 (4) (2006) 519–533.
[28] J. Henninger, B. Santoso, S. Hans, E. Durand, J. Moore, C. Mosimann, M. Brand, D. Traver, L. Zon, Clonal fate mapping quantifies the number of haematopoietic stem cells that arise during development, Nat. Cell Biol. 19 (1) (2017) 17–27.
[29] J. Livet, T.A. Weissman, H. Kang, R.W. Draft, J. Lu, R.A. Bennis, J.R. Sanes, J.W. Lichtman, Transgenic strategies for combinatorial expression of fluorescent proteins in the nervous system, Nature 450 (7166) (2007) 56–62.
[30] A. Amitai-Lange, E. Berkowitz, A. Altshuler, N. Dbayat, W. Nasser, E. Suss-Toby, B. Tiosano, R. Shalom-Feuerstein, A method for lineage tracing of corneal cells using multi-color fluorescent reporter mice, J. Vis. Exp. (106) (2015) 53370.
[31] L. Wang, R. Benedito, M.G. Bixel, D. Zeuschner, M. Stehling, L. Savendahl, J.J. Haigh, H. Snippert, H. Clevers, G. Breier, F. Kiefer, R.H. Adams, Identification of a clonally expanding haematopoietic compartment in bone marrow, EMBO J. 32 (2) (2013) 219–230.
[32] C.K. Chan, P. Lindau, W. Jiang, J.Y. Chen, L.F. Zhang, C.C. Chen, J. Seita, D. Sahoo, J.B. Kim, A. Lee, S. Park, D. Nag, Y. Gong, S. Kulkarni, C.A. Luppen, A.A. Theologis, D.C. Wan, A. DeBoer, E.Y. Seo, J.D. Vincent-Tompkins, K. Loh, G.G. Walmsley, D.L. Kraft, J.C. Wu, M.T. Longaker, I.L. Weissman, Clonal precursor of bone, cartilage, and hematopoietic niche stromal cells, Proc. Natl. Acad. Sci. U. S. A. 110 (31) (2013) 12643–12648.
[33] J.W. Tung, D.R. Parks, W.A. Moore, L.A. Herzenberg, L.A. Herzenberg, New approaches to fluorescence compensation and visualization of FACS data, Clin. Immunol. 110 (3) (2004) 277–283.
[34] H. Battifora, M. Kopinski, The influence of protease digestion and duration of fixation on the immunostaining of keratins. A comparison of formalin and ethanol fixation, J. Histochem. Cytochem. 34 (8) (1986) 1095–1100.
[35] A.S. Davis, A. Richter, S. Becker, J.E. Moyer, A. Sandouk, J. Skinner, J.K. Taubenberger, Characterizing and diminishing autofluorescence in formalin-fixed paraffin-embedded human respiratory tissue, J. Histochem. Cytochem. 62 (6) (2014) 405–423.
[36] A. Lorincz, Z. Nusser, Specificity of immunoreactions: the importance of testing specificity in each method, J. Neurosci. 28 (37) (2008) 9083–9086.
[37] B.S. Wilkins, Pitfalls in bone marrow pathology: avoiding errors in bone marrow trephine biopsy diagnosis, J. Clin. Pathol. 64 (5) (2011) 380–386.
[38] J.M. Fritschy, Is my antibody-staining specific? How to deal with pitfalls of immunohistochemistry, Eur. J. Neurosci. 28 (12) (2008) 2365–2370.
[39] V.A. Castania, J.W. Silveira, A.C. Issy, D.L. Pitol, M.L. Castania, A.D. Neto, E.A. Bel, H.L. Defino, Advantages of a combined method of decalcification compared to EDTA, Microsc. Res. Tech. 78 (2) (2015) 111–118.
[40] S.A. Gonzalez-Chavez, C. Pacheco-Tena, C.E. Macias-Vazquez, E. Luevano-Flores, Assessment of different decalcifying protocols on Osteopontin and Osteocalcin immunostaining in whole bone specimens of arthritis rat model by confocal immunofluorescence, Int. J. Clin. Exp. Pathol. 6 (10) (2013) 1972–1983.
[41] S.M. Hewitt, D.G. Baskin, C.W. Frevert, W.L. Stahl, E. Rosa-Molinar, Controls for immunohistochemistry: the Histochemical Society's standards of practice for validation of immunohistochemical assays, J. Histochem. Cytochem. 62 (10) (2014) 693–697.
[42] D.W. Dempster, J.E. Compston, M.K. Drezner, F.H. Glorieux, J.A. Kanis, H. Malluche, P.J. Meunier, S.M. Ott, R.R. Recker, A.M. Parfitt, Standardized nomenclature, symbols, and units for bone histomorphometry: a 2012 update of the report of the ASBMR Histomorphometry Nomenclature Committee, J. Bone Miner. Res. 28 (1) (2013) 2–17.
[43] S. Singbrant, M.R. Russell, T. Jovic, B. Liddicoat, D.J. Izon, L.E. Purton, N.A. Sims, T.J. Martin, V.G. Sankaran, C.R. Walkley, Erythropoietin couples erythropoiesis, B-lymphopoiesis, and bone homeostasis within the bone marrow microenvironment, Blood 117 (21) (2011) 5631–5642.
[44] J.M. Quach, M. Askmyr, T. Jovic, E.K. Baker, N.C. Walsh, S.J. Harrison, P. Neeson, D. Ritchie, P.R. Ebeling, L.E. Purton, Myelosuppressive therapies significantly increase pro-inflammatory cytokines and directly cause bone loss, J. Bone Miner. Res. 30 (2015) 886–897.
[45] L. Zhang, M. Chang, C.A. Beck, E.M. Schwarz, B.F. Boyce, Analysis of new bone, cartilage, and fibrosis tissue in healing murine allografts using whole slide imaging and a new automated histomorphometric algorithm, Bone Res. 4 (2016) 15037.
[46] R.J. van 't Hof, L. Rose, E. Bassonga, A. Daroszewska, Open source software for semi-automated histomorphometry of bone resorption and formation parameters, Bone 99 (2017) 69–79.
[47] O.R. Lopez-Vaca, D.A. Garzon-Alvarado, Spongiosa primary development: a biochemical hypothesis by Turing patterns formations, Comput. Math. Methods Med. 2012 (2012) 748302.
[48] C. Maes, Signaling pathways effecting crosstalk between cartilage and adjacent tissues: seminars in cell and developmental biology: the biology and pathology of cartilage, Semin. Cell Dev. Biol. 62 (2017) 16–33.
[49] D. Duarte, E.D. Hawkins, O. Akinduro, H. Ang, K. De Filippo, I.Y. Kong, M. Haltalli, N. Ruivo, L. Straszkowski, S.J. Vervoort, C. McLean, T.S. Weber, R. Khorshed, C. Pirillo, A. Wei, S.K. Ramasamy, A.P. Kusumbe, K. Duffy,

R.H. Adams, L.E. Purton, L.M. Carlin, C. Lo Celso, Inhibition of endosteal vascular niche remodeling rescues hematopoietic stem cell loss in AML, Cell Stem Cell 22 (1) (2018) 64–77 (e6).
[50] A.H. Zedan, S.G. Blavnsfeldt, T.F. Hansen, B.S. Nielsen, N. Marcussen, M. Pleckaitis, P.J.S. Osther, F.B. Sorensen, Heterogeneity of miRNA expression in localized prostate cancer with clinicopathological correlations, PLoS One 12 (6) (2017) e0179113.
[51] M. Takikita, S. Altekruse, C.F. Lynch, M.T. Goodman, B.Y. Hernandez, M. Green, W. Cozen, M. Cockburn, M. Sibug Saber, M. Topor, C. Zeruto, B. Abedi-Ardekani, M.E. Reichman, S.M. Hewitt, Associations between selected biomarkers and prognosis in a population-based pancreatic cancer tissue microarray, Cancer Res. 69 (7) (2009) 2950–2955.
[52] A. Zimpfer, S. Schonberg, A. Lugli, C. Agostinelli, S.A. Pileri, P. Went, S. Dirnhofer, Construction and validation of a bone marrow tissue microarray, J. Clin. Pathol. 60 (1) (2007) 57–61.
[53] R.C. Johnson, J.H. Kurzer, P.L. Greenberg, D. Gratzinger, Mesenchymal stromal cell density is increased in higher grade myelodysplastic syndromes and independently predicts survival, Am. J. Clin. Pathol. 142 (6) (2014) 795–802.
[54] K. Montgomery, S. Zhao, M. van de Rijn, Y. Natkunam, A novel method for making “tissue” microarrays from small numbers of suspension cells, Appl. Immunohistochem. Mol. Morphol. 13 (1) (2005) 80–84.
[55] U. Vogel, Overview on techniques to construct tissue arrays with special emphasis on tissue microarrays, Microarrays (Basel) 3 (2) (2014) 103–136.
[56] K.A. Limberger, L. Bogatyreva, R. Todorova, B. Herde, D. Hauschke, H.L. Pahl, M. Werner, K. Aumann, Tissue microarray technique is applicable to bone marrow biopsies of myeloproliferative neoplasms, Histochem. Cell Biol. 147 (1) (2017) 75–82.
[57] E. Gars, S.M. Yousry, D. Babu, J.H. Kurzer, T.I. George, D. Gratzinger, A replicable CD271+ mesenchymal stromal cell density score: bringing the dysfunctional myelodysplastic syndrome niche to the diagnostic laboratory, Leuk. Lymphoma 58 (7) (2017) 1730–1732.
[58] A. Tzankov, A.C. Pehrs, A. Zimpfer, S. Ascani, A. Lugli, S. Pileri, S. Dirnhofer, Prognostic significance of CD44 expression in diffuse large B cell lymphoma of activated and germinal centre B cell-like types: a tissue microarray analysis of 90 cases, J. Clin. Pathol. 56 (10) (2003) 747–752.
[59] C.P. Hans, D.D. Weisenburger, T.C. Greiner, R.D. Gascoyne, J. Delabie, G. Ott, H.K. Muller-Hermelink, E. Campo, R.M. Braziel, E.S. Jaffe, Z. Pan, P. Farinha, L.M. Smith, B. Falini, A.H. Banham, A. Rosenwald, L.M. Staudt, J.M. Connors, J.O. Armitage, W.C. Chan, Confirmation of the molecular classification of diffuse large B-cell lymphoma by immunohistochemistry using a tissue microarray, Blood 103 (1) (2004) 275–282.
[60] F. Naeim, F. Moatamed, M. Sahimi, Morphogenesis of the bone marrow: fractal structures and diffusion-limited growth, Blood 87 (12) (1996) 5027–5031.
[61] E. Flores-Figueroa, D. Gratzinger, Beyond the niche: myelodysplastic syndrome topobiology in the laboratory and in the clinic, Int. J. Mol. Sci. 17 (4) (2016) 553.
[62] M.D. Ewalt, D. Gratzinger, Selective quantitation of microvessel density reveals sinusoidal expansion in myelodysplastic syndromes, Leuk. Lymphoma 57 (12) (2016) 2923–2926.
[63] G. Nybakken, D. Gratzinger, Myelodysplastic syndrome macrophages have aberrant iron storage and heme oxygenase-1 expression, Leuk. Lymphoma 57 (8) (2016) 1893–1902.
[64] E. Flores-Figueroa, S. Varma, K. Montgomery, P.L. Greenberg, D. Gratzinger, Distinctive contact between CD34+ hematopoietic progenitors and CXCL12+ CD271+ mesenchymal stromal cells in benign and myelodysplastic bone marrow, Lab. Investig. 92 (9) (2012) 1330–1341.
[65] T. Takaku, D. Malide, J. Chen, R.T. Calado, S. Kajigaya, N.S. Young, Hematopoiesis in 3 dimensions: human and murine bone marrow architecture visualized by confocal microscopy, Blood 116 (15) (2010) e41–55.
[66] M.D. Cahalan, I. Parker, S.H. Wei, M.J. Miller, Two-photon tissue imaging: seeing the immune system in a fresh light, Nat. Rev. Immunol. 2 (11) (2002) 872–880.
[67] F. Progatzky, M.J. Dallman, C. Lo Celso, From seeing to believing: labelling strategies for in vivo cell-tracking experiments, Interface Focus 3 (3) (2013) 20130001.
[68] A.T. Hooper, J.M. Butler, D.J. Nolan, A. Kranz, K. Iida, M. Kobayashi, H.G. Kopp, K. Shido, I. Petit, K. Yanger, D. James, L. Witte, Z. Zhu, Y. Wu, B. Pytowski, Z. Rosenwaks, V. Mittal, T.N. Sato, S. Rafii, Engraftment and reconstitution of hematopoiesis is dependent on VEGFR2-mediated regeneration of sinusoidal endothelial cells, Cell Stem Cell 4 (3) (2009) 263–274.
[69] M. Dominici, V. Rasini, R. Bussolari, X. Chen, T.J. Hofmann, C. Spano, D. Bernabei, E. Veronesi, F. Bertoni, P. Paolucci, P. Conte, E.M. Horwitz, Restoration and reversible expansion of the osteoblastic hematopoietic stem cell niche after marrow radioablation, Blood 114 (11) (2009) 2333–2343.
[70] M.J. Kiel, O.H. Yilmaz, T. Iwashita, O.H. Yilmaz, C. Terhorst, S.J. Morrison, SLAM family receptors distinguish hematopoietic stem and progenitor cells and reveal endothelial niches for stem cells, Cell 121 (7) (2005) 1109–1121.
[71] H. Oguro, L. Ding, S.J. Morrison, SLAM family markers resolve functionally distinct subpopulations of hematopoietic stem cells and multipotent progenitors, Cell Stem Cell 13 (1) (2013) 102–116.
[72] E.M. Pietras, D. Reynaud, Y.A. Kang, D. Carlin, F.J. Calero-Nieto, A.D. Leavitt, J.M. Stuart, B. Gottgens, E. Passegue, Functionally distinct subsets of lineage-biased multipotent progenitors control blood production in normal and regenerative conditions, Cell Stem Cell 17 (1) (2015) 35–46.
[73] Y. Kunisaki, I. Bruns, C. Scheiermann, J. Ahmed, S. Pinho, D. Zhang, T. Mizoguchi, Q. Wei, D. Lucas, K. Ito, J.C. Mar, A. Bergman, P.S. Frenette, Arteriolar niches maintain haematopoietic stem cell quiescence, Nature 502 (7473) (2013) 637–643.
[74] W. Denk, J. Strickler, W. Webb, Two-photon laser scanning fluorescence microscopy, Science 248 (4951) (1990) 73–76.
[75] W. Denk, K. Svoboda, Photon upmanship: why multiphoton imaging is more than a gimmick, Neuron 18 (3) (1997) 351–357.
[76] F. Helmchen, W. Denk, Deep tissue two-photon microscopy, Nat. Methods 2 (12) (2005) 932–940.
[77] K. König, Multiphoton microscopy in life sciences, J. Microsc. 200 (2) (2000) 83–104.
[78] C. Lo Celso, H.E. Fleming, J.W. Wu, C.X. Zhao, S. Miake-Lye, J. Fujisaki, D. Cote, D.W. Rowe, C.P. Lin, D.T. Scadden, Live-animal tracking of individual haematopoietic stem/progenitor cells in their niche, Nature 457 (7225) (2009) 92–96.
[79] C. Halin, J.R. Mora, C. Sumen, U.H. von Andrian, In vivo imaging of lymphocyte trafficking, Annu. Rev. Cell Dev. Biol. 21 (2005) 581–603.
[80] W.R. Zipfel, R.M. Williams, W.W. Webb, Nonlinear magic: multiphoton microscopy in the biosciences, Nat. Biotechnol. 21 (11) (2003) 1369–1377.
[81] G. Tjin, P. Xu, S.H. Kable, E.P. Kable, J.K. Burgess, Quantification of collagen I in airway tissues using second harmonic generation, J. Biomed. Opt. 19 (3) (2014) 36005.
[82] G. Tjin, G. Cox, Application of second harmonic imaging microscopy in biological studies, Encyclopedia of Analytical Chemistry, John Wiley & Sons, Ltd, 2006.
[83] R.A. Khorshed, E.D. Hawkins, D. Duarte, M.K. Scott, O.A. Akinduro, N.M. Rashidi, M. Spitaler, C. Lo Celso, Automated identification and localization of hematopoietic stem cells in 3D intravital microscopy data, Stem Cell Rep. 5 (1) (2015) 139–153.
[84] N.M. Rashidi, M.K. Scott, N. Scherf, A. Krinner, J.S. Kalchschmidt, K. Gounaris, M.E. Selkirk, I. Roeder, C. Lo Celso, In vivo time-lapse imaging shows diverse niche engagement by quiescent and naturally activated hematopoietic stem cells, Blood 124 (1) (2014) 79–83.
[85] M.K. Scott, O. Akinduro, C. Lo Celso, In vivo 4-dimensional tracking of hematopoietic stem and progenitor cells in adult mouse calvarial bone marrow, J. Vis. Exp. (91) (2014) e51683.
[86] F. Lassailly, K. Foster, L. Lopez-Onieva, E. Currie, D. Bonnet, Multimodal imaging reveals structural and functional heterogeneity in different bone marrow compartments: functional implications on hematopoietic stem cells, Blood 122 (10) (2013) 1730–1740.
[87] M.G. Bixel, A.P. Kusumbe, S.K. Ramasamy, K.K. Sivaraj, S. Butz, D. Vestweber, R.H. Adams, Flow dynamics and HSPC homing in bone marrow microvessels, Cell Rep. 18 (7) (2017) 1804–1816.
[88] J.C. Voyta, D.P. Via, C.E. Butterfield, B.R. Zetter, Identification and isolation of endothelial cells based on their increased uptake of acetylated-low density lipoprotein, J. Cell Biol. 99 (6) (1984) 2034–2040.
[89] S.P. Sorokin, R.F. Hoyt Jr., Macrophage development: I. Rationale for using Griffonia simplicifolia isolectin B4 as a marker for the line, Anat. Rec. 232 (4) (1992) 520–526.
[90] J. Secklehner, C. Lo Celso, L.M. Carlin, Intravital microscopy in historic and contemporary immunology, Immunol. Cell Biol. 95 (6) (2017) 506–513.
[91] Y. Xie, T. Yin, W. Wiegraebe, X.C. He, D. Miller, D. Stark, K. Perko, R. Alexander, J. Schwartz, J.C. Grindley, J. Park, J.S. Haug, J.P. Wunderlich, H. Li, S. Zhang, T. Johnson, R.A. Feldman, L. Li, Detection of functional haematopoietic stem cell niche using real-time imaging, Nature 457 (7225) (2009) 97–101.
[92] S. Mendez-Ferrer, D. Lucas, M. Battista, P.S. Frenette, Haematopoietic stem cell release is regulated by circadian oscillations, Nature 452 (7186) (2008) 442–447.
[93] A. Kohler, V. Schmithorst, M.D. Filippi, M.A. Ryan, D. Daria, M. Gunzer, H. Geiger, Altered cellular dynamics and endosteal location of aged early hematopoietic progenitor cells revealed by time-lapse intravital imaging in long bones, Blood 114 (2) (2009) 290–298.
[94] L.A. Pitt, A.N. Tikhonova, H. Hu, T. Trimarchi, B. King, Y. Gong, M. Sanchez-Martin, A. Tsirigos, D.R. Littman, A.A. Ferrando, S.J. Morrison, D.R. Fooksman, I. Aifantis, S.R. Schwab, CXCL12-producing vascular endothelial niches control acute T cell leukemia maintenance, Cancer Cell 27 (6) (2015) 755–768.
[95] N. Asada, Y. Katayama, M. Sato, K. Minagawa, K. Wakahashi, H. Kawano, Y. Kawano, A. Sada, K. Ikeda, T. Matsui, M. Tanimoto, Matrix-embedded osteocytes regulate mobilization of hematopoietic stem/progenitor cells, Cell Stem Cell 12 (6) (2013) 737–747.
[96] D. Lewandowski, V. Barroca, F. Duconge, J. Bayer, J.T. Van Nhieu, C. Pestourie, P. Fouchet, B. Tavitian, P.H. Romeo, In vivo cellular imaging pinpoints the role of reactive oxygen species in the early steps of adult hematopoietic reconstitution, Blood 115 (3) (2010) 443–452.
[97] I.B. Mazo, J.C. Gutierrez-Ramos, P.S. Frenette, R.O. Hynes, D.D. Wagner, U.H. von Andrian, Hematopoietic progenitor cell rolling in bone marrow microvessels: parallel contributions by endothelial selectins and vascular cell adhesion molecule 1, J. Exp. Med. 188 (3) (1998) 465–474.
[98] R. Turcotte, C. Alt, L.J. Mortensen, C.P. Lin, Characterization of multiphoton microscopy in the bone marrow following intravital laser osteotomy, Biomed. Opt. Express 5 (10) (2014) 3578–3588.
[99] K. Foster, F. Lassailly, F. Anjos-Afonso, E. Currie, K. Rouault-Pierre, D. Bonnet, Different motile behaviors of human hematopoietic stem versus progenitor cells at the osteoblastic niche, Stem Cell Rep. 5 (5) (2015) 690–701.
[100] M.A. Lawson, M.M. McDonald, N. Kovacic, W. Hua Khoo, R.L. Terry, J. Down, W. Kaplan, J. Paton-Hough, C. Fellows, J.A. Pettitt, T. Neil Dear, E. Van Valckenborgh, P.A. Baldock, M.J. Rogers, C.L. Eaton, K. Vanderkerken, A.R. Pettit, J.M. Quinn, A.C. Zannettino, T.G. Phan, P.I. Croucher, Osteoclasts control reactivation of dormant myeloma cells by remodelling the endosteal niche, Nat. Commun. 6 (2015) 8983.
[101] M. Acar, K.S. Kocherlakota, M.M. Murphy, J.G. Peyer, H. Oguro, C.N. Inra, C. Jaiyeola, Z. Zhao, K. Luby-Phelps, S.J. Morrison, Deep imaging of bone marrow

shows non-dividing stem cells are mainly perisinusoidal, Nature 526 (2015) 126.
[102] D.S. Richardson, J.W. Lichtman, Clarifying tissue clearing, Cell 162 (2) (2015) 246–257.
[103] D.L. Coutu, K.D. Kokkaliaris, L. Kunz, T. Schroeder, Multicolor quantitative confocal imaging cytometry, Nat. Methods 15 (2017) 39.
[104] C. Nombela-Arrieta, G. Pivarnik, B. Winkel, K.J. Canty, B. Harley, J.E. Mahoney, S.Y. Park, J. Lu, A. Protopopov, L.E. Silberstein, Quantitative imaging of haematopoietic stem and progenitor cell localization and hypoxic status in the bone marrow microenvironment, Nat. Cell Biol. 15 (5) (2013) 533–543.
[105] E. Nolan, P. Savas, A.N. Policheni, P.K. Darcy, F. Vaillant, C.P. Mintoff, S. Dushyanthen, M. Mansour, J.B. Pang, S.B. Fox, C. Kathleen Cuningham, Foundation Consortium for Research into Familial Breast, C.M. Perou, J.E. Visvader, D.H.D. Gray, S. Loi, G.J. Lindeman, Combined immune checkpoint blockade as a therapeutic strategy for BRCA1-mutated breast cancer, Sci. Transl. Med. 9 (393) (2017).
[106] Q. Chang, O.I. Ornatsky, I. Siddiqui, A. Loboda, V.I. Baranov, D.W. Hedley, Imaging mass cytometry, Cytometry A 91 (2) (2017) 160–169.
[107] Q. Chang, O. Ornatsky, D. Hedley, Staining of frozen and formalin-fixed, paraffin-embedded tissues with metal-labeled antibodies for imaging mass cytometry analysis, Curr. Protoc. Cytom. 82 (2017) 12471–12478.
[108] C. Giesen, H.A. Wang, D. Schapiro, N. Zivanovic, A. Jacobs, B. Hattendorf, P.J. Schuffler, D. Grolimund, J.M. Buhmann, S. Brandt, Z. Varga, P.J. Wild, D. Gunther, B. Bodenmiller, Highly multiplexed imaging of tumor tissues with subcellular resolution by mass cytometry, Nat. Methods 11 (4) (2014) 417–422.
[109] D. Schulz, V.R.T. Zanotelli, J.R. Fischer, D. Schapiro, S. Engler, X.K. Lun, H.W. Jackson, B. Bodenmiller, Simultaneous multiplexed imaging of mRNA and proteins with subcellular resolution in breast cancer tissue samples by mass cytometry, Cell Syst. 6 (1) (2018) 25–36 (e5).
[110] A. Mavropoulos, B. Allo, M. He, E. Park, D. Majonis, O. Ornatsky, Simultaneous detection of protein and mRNA in Jurkat and KG-1a cells by mass cytometry, Cytometry A 91 (12) (2017) 1200–1208.